CHALMERS
UNIVERSITY OF TECHNOLOGY

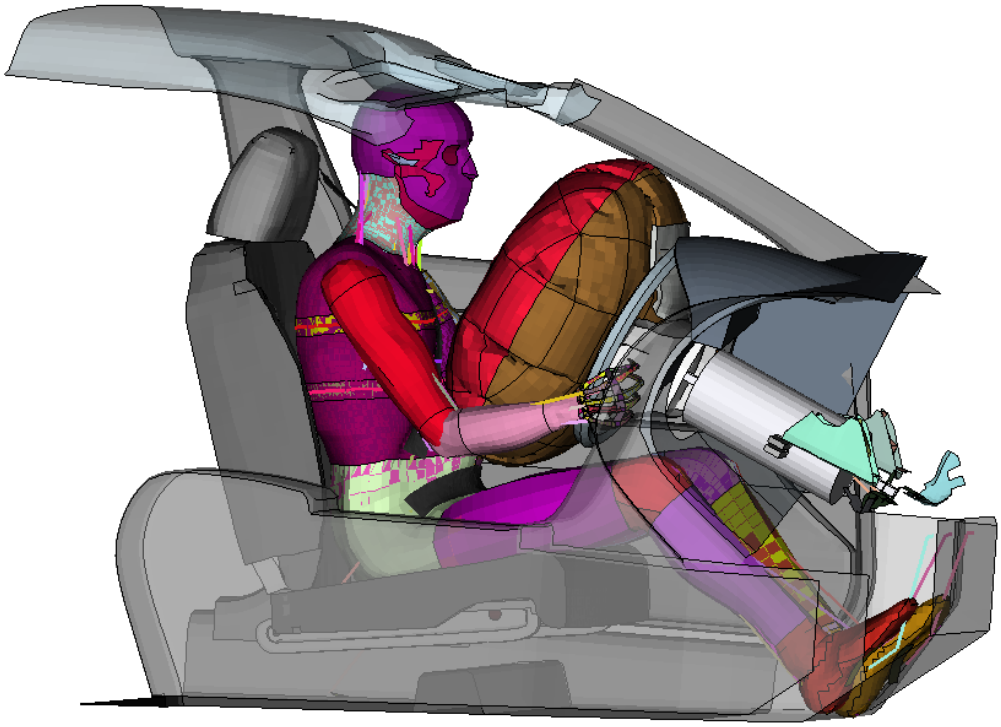

Vehicle crash reconstructions using FE human body model to improve injury predictions

Master's thesis in Applied Mechanics

PALOMA MUÑIZ FERNÁNDEZ
ILIJA TODOROVIC

Department of Mechanics and Maritime Sciences
CHALMERS UNIVERSITY OF TECHNOLOGY
Gothenburg, Sweden 2020

MASTER'S THESIS 2020:32

Vehicle crash reconstructions using FE human body model to improve injury predictions

Paloma Muñiz Fernández, Ilija Todorovic

Department of Mechanics and Maritime Sciences

Division of Vehicle Safety

CHALMERS UNIVERSITY OF TECHNOLOGY

Göteborg, Sweden 2020

Vehicle crash reconstructions using FE human body model to improve injury predictions

Paloma Muñiz Fernández, Ilija Todorovic

Master's Thesis 2020:32

Department of Mechanics and Maritime Sciences

Division of Vehicle Safety

Chalmers University of Technology

SE-412 96 Göteborg
Sweden
Telephone: + 46 (0)31-772 1000

Cover:

SAFER HBM positioned in the simplified vehicle model.

Department of Mechanics and Maritime Sciences

Göteborg, Sweden 2020-06-03

Vehicle crash reconstructions using FE human body model to improve injury predictions

Master's thesis in Applied mechanics

Paloma Muñiz Fernández, Ilija Todorovic

Department of Mechanics and Maritime Sciences
Division of Vehicle Safety
Chalmers University of Technology

Abstract

FE Human Body Models (HBMs) represent an important researching tool for assessing occupant injuries on tissue level. Although prior research has overtime led to considerable improvements, further validation of today's HBMs is needed in order to ensure model biofidelity. In this thesis, SAFER HBM v9 is validated through reconstructions of 11 real world motor vehicle crashes with known injury outcomes.

The SAFER HBM is positioned into a generic simplified vehicle model (SVM) by using Marionette method. The SAFER HBM is then scaled in four of the reconstruction cases in order to better match occupant statures. After the model pre-set in ANSA, simulations are run in the FE- solver LS-DYNA and the obtained results are analyzed in the LS-PrePost and META. The injury validation is based on comparing simulation results with the reported real-world injury outcomes of head, ribcage and lumbar spine for the selected reconstruction cases. In particular, AIS2+ risk for concussion is estimated considering 1st Principal Green St Venant strain in corpus callosum, gray matter and white matter of the KTH brain model. Moreover, AIS2+ probability fracture risk is estimated for the entire ribcage based on strain-based probabilistic method with age adjustment. In addition, forces and moments are analyzed in lumbar spine vertebrae and are related to compression fracture injuries based on existing thresholds suggested in previous studies.

The concussion results show that the model significantly underestimates the probability for concussion for the cases with reported severe head injuries. The preliminary conclusion from the evaluated risk for rib fractures is that the model in average overpredicts the AIS2+ probability risk. The applied lumbar criterion shows a progressively increased fracture probability risk from vertebra L1 to L5, regardless of the real-world fracture outcome. When considering lumbar compression forces independent to other loads, the cases where lumbar fractures where reported indicates on average higher compression forces in comparison to non-fracture cases.

Finally, improvements are suggested for the implemented validation methods, in order to increase reliability for the future injury predictions.

Keywords: Human Body Model, Finite element analysis, Vehicle crash reconstructions, Passive safety, Biomechanics, Injury validation, Frontal impact, LS-DYNA.

Acknowledgements

This master thesis is carried out at the Department of Mechanics and Maritime Sciences as a joint project between Chalmers University of Technology, Autoliv and Volvo Cars. We would like to thank our examiner Johan Davidsson and PhD employees at Division of Vehicle Safety for support at several occasions throughout the project. A special thanks to Karl-Johan Larsson, for sharing his knowledge about HBM positioning method. We would also like to express a great thanks to the supervisor of the project, Johan Iraeus, for his guidance and consultations. Furthermore, we would like to address our gratitude to DynaMore Nordic for opportunity to attend the introductory course in LS-DYNA. Finally, we would like to thank our student mates at the division of Vehicle Safety for exchanged ideas and valuable conversations.

Gothenburg June 2020-06-03

Paloma Muñiz Fernández, Ilija Todorovic

Nomenclature

AAAM	Association for the Advancement of Automotive Medicine
AIS	Abbreviated Injury Scale
ATDs	Anthropomorphic test devices
CAE	Computer Aided Engineering
CDC	Collision Deformation Classification
CIREN	Crash Injury Research and Engineering Network
COG	Center of Gravity
CSF	Cerebrospinal fluid
CT	Computer tomography
DAI	Diffuse Axonal Injury
DOE	Design of experiments
DDM	Dilatation Damage Measure
EDR	Event data recorder
FE	Finite element
GHBMC	Global Human Body Model Consortium
HBMs	Human body models
HIC	Head injury criterion
HUMOS	Human model for safety
LSTC	Livermore Software Technology Corporation
MOI	Mechanism of Injury
MPP	Massively Parallel Processing
MVCs	Motor vehicle crashes
NASS-CDS	National Automotive Sampling System Crashworthiness Data System
NHTSA	National Highway Traffic Safety Administration
NFL	National Football League
NFR	Number of fractured ribs
PB	Poisson Binomial
PDOF	Principal Direction Of Force
PMHS	Post mortem human subjects
SVM	Simplified Vehicle Model
TBI	Traumatic brain injury
THUMS	Total HUman Model for Safety
TTI	Thoracic trauma index
VCC	Volvo Cars Corporation
WHO	World Health Organisation

Contents

List of figures

List of tables

1 Introduction

In the past decades, great efforts have been made worldwide for occupant protection enhancements associated with motor vehicle crashes (MVCs). Progress of reducing occupant fatalities and injuries has been achieved partly by introducing legislations and safety standards for roads and vehicles but also through improvements in vehicle crashworthiness and technical advancements of restraint systems [1], [2]. Nevertheless, according to World Health Organisation (WHO), injuries and deaths associated with road traffic crashes remain a serious problem globally, with the road traffic crashes representing the eight leading cause of death globally, claiming more than 1.35 million lives each year and causing up to 50 million injuries [1].

Currently, occupant protection assessment regarding passive safety is based extensively on anthropomorphic test devices (ATDs), commonly referred to as crash test dummies. Although frequently used for evaluating motor vehicle crash scenarios in both virtual simulations and physical environments, crash test dummies represent a limitation in vehicle safety assessment due to their simplified design of a human anatomy. For this reason, vehicle safety development is increasingly relying on the Finite element (FE) Human body models (HBMs) used as a complement to the ATDs [3]. Unlike crash test dummies, HBMs are generally designed to replicate the human anatomy and material properties with detailed skeleton, internal organs, and soft tissues including active muscle response [4]. This makes it possible to address injury at a more detailed level, such as local chest injuries, which provides an increased understanding of injuries sustained by occupants in vehicle crashes. Moreover, HBMs are capable of predicting human kinematics and injury risks in oblique crashes which in turn contributes to higher biofidelity of HBMs than that of ATDs [3] [5].

With advanced computer-based simulation capacity, the development of HBMs has led to several different models widely used in the research context of vehicle safety. Today, there are two major FE HBMs in use representing average-sized males, namely Total HUman Model for Safety (THUMS) AM50 and the Global Human Body Model Consortium (GHBMC) M50-O model [3]. However, it has been pointed out that these two major HBMs have shown lack of capability to correctly predict injury validations under certain loading conditions. For example,

it was shown that both HBMs under-predicted the number of rib fractures compared to the outcome of the cadaver tests [6].

As HBMs are becoming a very useful researching tool to predict detailed pre- and in-crash occupant response it is of vital importance to ensure the model validity. Establishing an adequate level of biofidelity through model validation extends possibilities for development of future advanced restraint systems leading to improved occupant safety.

1.1 Background

In the current project, the SAFER HBM v9 will be used. This model originates from THUMS AM50 v3 and has been modified in several projects [3], [7]. There are several previously performed studies on validation of SAFER HBM v9. For example, in study [3] the generic ribcage of the model was validated implementing three different validation methods of different complexity: anterior-posterior rib bending tests; rigid impactor table-top test; and a frontal sled test. In this way kinetic, kinematics and strain distribution of the ribcage was evaluated. Another example is study [5], a multi-scale validation for predicting the risk for an occupant to sustain two or more rib fractures, by means of a probabilistic rib fracture prediction method. Beside sled test with post mortem human subjects (PMHS) and rigid impactor table-top test the study considered also so-called detailed accident reconstructions and population-based reconstructions. The results generally indicated that the risk of fractured ribs was successfully predicted.

Since only 22 detailed crash reconstructions have been carried out until currently, there is a need for additional reconstructions to further strengthen the model validity and thus broaden the confidence in the capability of the model.

1.2 Purpose

The purpose of this master thesis is to strengthen the validity of a SAFER HBM v9 by creating 11 virtual crash reconstructions from real life crashes. In particular, the aim is to evaluate the capability of the SAFER HBM v9 to predict three types of injuries. More specifically, injury validation of rib fractures, concussion

and lumbar spine fracture are being considered, since the SAFER HBM v9 is targeting injury risk predictions for these areas.

1.3 Limitations

Only frontal crashes are included with intention to analyse in-crash phase of the collisions. 4 out of 11 selected cases include female drivers and most of the occupants are of different ages. Despite this variety, the SAFER HBM will be implemented without morphing. Instead, scaling will be used to better represent occupants with largest deviation in size.

The SVM is used to represent different vehicles of the reconstruction cases. The initial and boundary conditions of the crash parameters are predefined. The boundary conditions were prescribed based on the event data recorder (EDR), accounting only longitudinal crash pulse.

When it comes to injury validation of the head and the thorax, injury criteria choices are narrowed to tissue-level assessment, strains in particular. This is based on suggestions in previous studies covered in the literature overview.

For the head, only concussion injury is assessed. For the rib fracture validation, injury probability is based on the ribcage as a whole, neither an exact number of rib fractures nor exact location of these is assessed. For the spine, injury is validated based exclusively on forces and moments measured in lumbar vertebras.

1.4 Crash case selection

The 11 considered crash cases in the current study have been used in two previous studies performed by Virginia Tech, [8] and [9]. The aim of these studies was to, by the means of finite element MVC reconstructions, investigate the risks of thoracolumbar spine fractures and driver lower extremity injuries. The cases for FE reconstruction were selected from the NASS-CDS and CIREN databases as shown in Table 1.1. The table also shows driver characteristics, case ID, Principal Direction Of Force (PDOF) and longitudinal Delta-V measured with an event data recorder (EDR) for each vehicle - see section 2.1.2 for clarification of here

mentioned terms. All eleven selections are full-frontal crashes with a Collision Deformation Classification (CDC) code of "FDEW" (denoting categorisation of vehicle damage) [9]. Moreover, all cases involve belted drivers and frontal airbag deployment. According to [9], selections were made with intention to include a broad range of common Abbreviated Injury Scale (AIS) 2+ injuries involving rib fractures and thoracolumbar fractures and head injuries.

Table 1.1: 11 selected cases for FE reconstruction with vehicle information and driver characteristics.

Case Nr	Database	Case ID	Vehicle	PDOF (°)	DeltaV (km/h)	Age	Sex	Mass (kg)	Height (cm)
Case 1	CIREN	359501964	Honda Civic (2012)	0	56.3	67	F	66	165
Case 2	CIREN	431354202	Toyota Corolla (2007)	350	54.5	57	M	71	165
Case 3	CIREN	317349598	Lexus ES350 (2008)	10	69.7	43	M	88	175
Case 4	CIREN	128763	Chevrolet Malibu (2006)	350	61.1	69	M	82	173
Case 5	NASS-CDS	437010451	Chevrolet Silverado (2005)	0	59.9	23	M	79	175
Case 6	CIREN	588557622	Toyota Solara (2007)	350	31.8	50	F	67	173
Case 7	CIREN	338103538	Toyota Camry (2010)	10	64.0	21	F	64	160
Case 8	NASS-CDS	126015217	Chevrolet Cavalier (2002)	0	49.4	18	M	64	175
Case 9	CIREN	385119464	Chevrolet Cobalt (2006)	350	42.6	80	M	77	183
Case 10	CIREN	359544180	Ford Escape (2012)	0	49.9	86	M	84	175
Case 11	NASS-CDS	784014636	Hummer H3 (2007)	350	57.4	50	F	86	173

1.5 Simulation model

The 11 provided simulation models used in this study consist of a Simplified Vehicle Model (SVM) and the SAFER HBM. The SVMs have been tuned to mimic a certain vehicle-specific response as described below.

1.5.1 Simplified Vehicle Model (SVM)

The eleven considered reconstructions include different type of vehicles. However, in this study a FE Simplified Vehicle Model (SVM) will be used for simulation of all the cases. The SVM is a generic vehicle geometry profile developed from combined laser scans of 14 different vehicle interior models validated on a population of NASS/CDS frontal crashes [10]. The geometry of the final interior is simplified by removing air vents, buttons, and displays including only major components such as b-pillar, door trim, instrument panel, center console, steering wheel, pedals and a seat with the seat suspension springs and a foam cushion, see Figure 1.1. Additionally, the model is supplemented with the roof, the door and the windshield for the sake of visualization. Most of the components are modeled as rigid parts, except for the instrument panel, the lower part of steering wheel, the airbag, the seat and the seat belt.

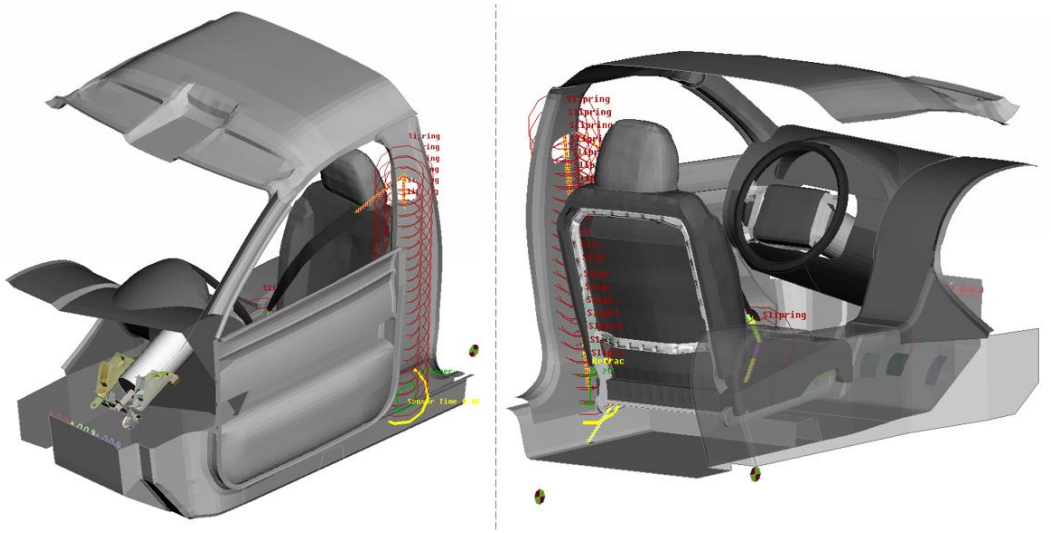

Figure 1.1: Illustration of the SVM viewed from two different angles.

The SVM was previously developed by Iraeus, J. and Lindquist, M [10] and was further modified in study [11] to include a seat belt with a pretensioner and

retractor, but also frontal and knee airbags. In addition, the SVM was tuned by using a semi-automated approach as described in [11]. More specifically, in order to represent a vehicle-specific response, a so-called Latin hypercube design of experiments (DOE) was performed, meaning that multiply independent parameters were varied to optimize the restraint systems, to match the vehicle of study.

1.5.1.1 Restraint system in the SVM

The provided SVM contains several restraint systems, with the collapsible steering column being one of them. The collapsible steering column is responsible for absorbing energy in frontal car crashes. In the SVM, the mechanism of the steering column is basically consisting of two cylinders that are dimensioned so that in the event of an accident, one cylinder fits inside the other, and the steering wheel retracts absorbing the energy of the impact and considerably reducing the risk of head or rib cage injury.

Furthermore, a driver airbag (DAB) is placed in the steering wheel. It is meant to inflate under a certain pressure and during a short period of time [12]. The frontal steering wheel airbag is modelled in all the 11 crash cases. In addition, case 3 and case 7 are equipped with a knee airbag. The knee airbag is divided into multiple layers and modeled as simplified foam padding with stress versus strain response [8]. Both types of frontal airbags can be seen in Figure 1.2.

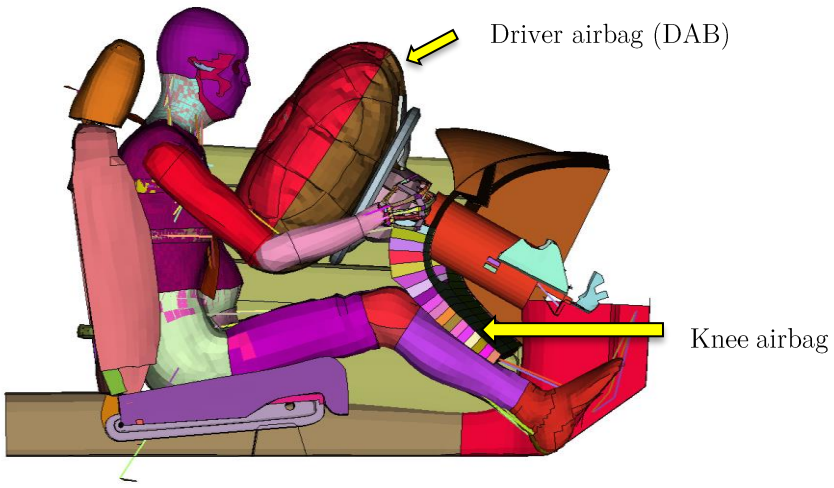

Figure 1.2: DAB and knee airbag in case 7.

Additionally, a 3-point seatbelt with a pretensioner and a load limiting retractor is included in each reconstruction case. A retractor, commonly composed of spring-loaded reels with inertial locking mechanism, is used to remove initial belt slack. The pretensioner is integrated into the retractor and is used to tighten the shoulder belt within milliseconds after the crash has been detected. The modelled seatbelt of the SVM is shown in Figure 1.3 on the left, and an illustration example of real seatbelt components is shown on the right for clarity. The seatbelt is modeled partly as 1D elements and partly as 2D lap and shoulder webbing shell elements. Width of the webbing entities is 48 mm and its material is MAT_PIECEWISE_LINEAR_PLASTICITY. Each case has customized D-ring height for the seat belt and steering column position with varying angels.

Figure 1.3: a) Initial 3-point seat belt model with sliprings, a retractor and a pretensioner and b) illustration of real belt components, image adapted with permission from [13].

1.5.2 SAFER HBM v9

The SAFER HBM v9.0, with 175 cm height and 77 weight, is representing a 50-percentile adult male, see Figure 1.4. Model units are millimeters (mm), milliseconds (ms), kilograms (kg) and thus consequently kN and GPa.

Compared to the original THUMS AM50 v3 the SAFER HBM has a modified cervical and lumbar spine, a remodeled rib-cage, and new material definitions for skin and fat [14]. The KTH head model developed at the Royal Institute of Technology in Stockholm has been inserted and consists of all the main

components of the head, such as scalp, skull, brain, cerebrospinal fluid (CSF), the meninges and eleven pairs of the largest parasagittal bridging veins [2] [15].

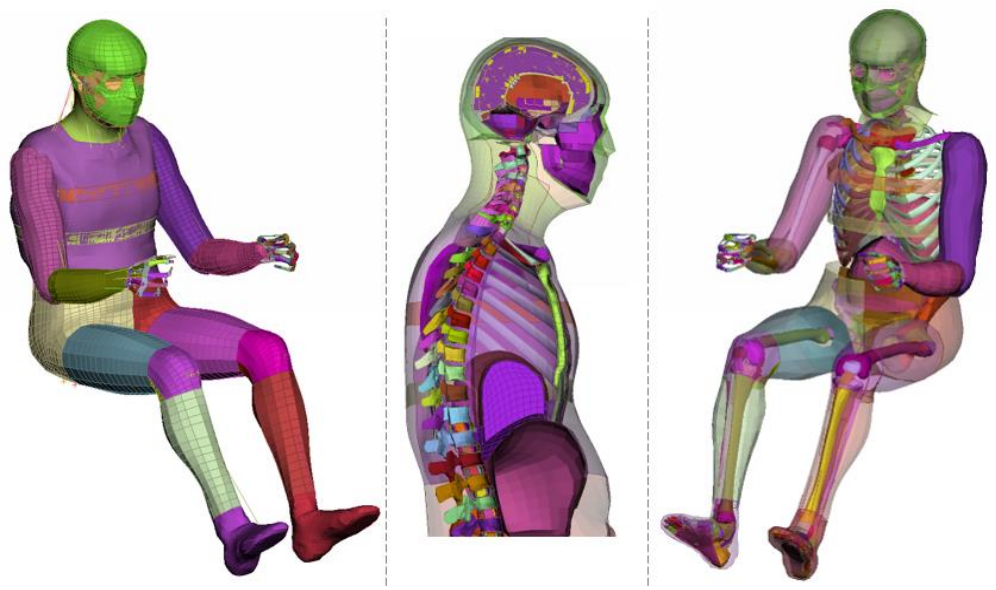

Figure 1.4: Three different views of SAFER HBM v9 including transparent skin surfaces and a section cut for visibility of the model internal parts such as bones and brain tissues.

1.5.3 Simulation software

The simulations are performed in the FE solver LS-DYNA MM R9.3.0 rev 119543 along with the pre-processor ANSA v.19.1.5 for preparing the solver input files and the post-processors META v.19.1.5 and LS-PrePost, for analysing the results. All FE simulation runs were performed on a (Hebbe) cluster computer.

1.5.3.1 LS-DYNA

The FE-solver LS-DYNA is suitable for a wide range of applications in automotive, biomechanics, aerospace, manufacturing, civil engineering and electronics etc [16]. The software includes specialized entities with capabilities to model safety restraint systems such as seat belts with pretensioners and retractors but also airbags and their inflation [17]. This makes LS-DYNA suitable for crash analysis. The solver consists of single executable file and is entirely command line driven, with no graphical user interface. Input files are in ASCII format and can be created using a text editor or with the aid of a graphical preprocessor such as LS-PrePost or ANSA.

1.5.3.2 ANSA

The pre-processor ANSA is an advanced multidisciplinary Computer Aided Engineering (CAE) tool compatible with LS-DYNA. ANSA contains a wide range of features and tools accommodated in an integrated environment with capability of handling both CAD geometries and FE model data. Specialized features for the crash safety analysis are included for solving sophisticated positioning problems, defining airbags, modelling seatbelt and morphing to modify existing designs [18].

1.5.3.3 META and LS-PrePost

META is a high performance multi-disciplinary CAE post-processor with advanced graphical tool along with numerous other tools capable of handling large, multiple model data with possibility to make correlation studies on loaded results, create plots and animations, extract reports and more [19].

LS PrePost is a pre- and post-processor intended specifically for LS DYNA.

2 Theory

This chapter is intended to introduce the reader with the theoretical parts that need to be acknowledged in order to obtain increased understanding for implemented methodology and obtained results. The chapter is introduced with description of how data for MVC reconstructions is gathered for further implementation of reconstructions into FE analysis. This is followed by an overview of previous validation studies of HBMs using real life crashes. Next, injury description of the head, thorax and lumbar spine is briefly explained, including an overview of anatomy, injury severity, injury mechanism and injury criteria.

2.1 MVC reconstruction

This section desribes MVC investigation process, CIREN and NASS-CDS databases, including description of the Abbreviated Injury Scale (AIS) and virtual FE reconstructions of real world MVCs.

2.1.1 MVC investigation process

Crash reconstructions are based on the gathered information of collision accidents by investigating the environment where a collision took place and by documenting potential injuries of the involved passengers. In-depth investigations of MVCs have been implemented for more than five decades, with the purpose to collect data valuable for injury mitigation and assessment of restraint system and crashworthiness [20]. The process of data collection involves most often site surveying, use of photography and 3D laser scanning, observation of tire marks and collecting other pertinent physical evidence available after the crash event that might be contributing factors to draw conclusions of the causes of the collision [21], [22]. More importantly, the collision vehicle is examined. By observing direction of the structural deformation of the vehicle provides better understanding of the collision type. Additionally, vehicles event data recorder (EDR) might be present in the vehicle, and the recorded signals (vehicle impact speed etc) downloaded [21]. One of the challenges is to determine the vehicle's

pre-impact velocity and trajectory [23], which may be established by application of engineering principles, using the laws of energy and conservation of linear momentum analysis [20], [24].

2.1.2 CIREN and NASS-CDS databases

Findings of an accident scene investigation are summarized in a traffic collision report by an expert crash analyst and the results are being incorporated into injury databases [20]. The Crash Injury Research and Engineering Network (CIREN) database, led by the National Highway Traffic Safety Administration (NHTSA), is example of one source of real-world MVC data. The CIREN database combines collected data from each field investigation of crashes with medical data from of a sample of injured patients to determine injury causation [25]. Once identified, the injuries are coded into the research database [22]. However, there might be some uncertainties on the exact mechanics of documented injury due to the lack of available data at the crash scene [11]. For example, occupant sitting position might be uncertain due to the fact that documented data is collected in the post-crash stage and not at the time when a crash occurred [26].

Another example of a database used for assessing injury causation is the National Automotive Sampling System–Crashworthiness Data System (NASS-CDS) [20]. In the present study, three of the selected real-world vehicle crashes are based on NASS-CDS database and the rest on CIREN database. One difference between these databases is that CIREN considers rather severely injured occupants who are admitted to a level one trauma hospital. On the other hand, NASS-CDS cases commonly deals with other medical criteria, cases with lower severity injury levels.

A commonly used metric in crash databases that describes injury severity is Delta-V, which can be seen as the total change in vehicle velocity over the duration of the crash event (between the pre-impact and post impact crash phase) [27]. PDOF is another important metric defined as the direction of the resultant of all impact forces acting on the vehicle during the collision phase [28]. The PDOF is estimated by a crash examiner and is typically defined in terms of degrees or hours of a clock dial, where 12 o'clock is oriented toward the front of the vehicle, corresponding to 0 degrees, Figure 2.1.

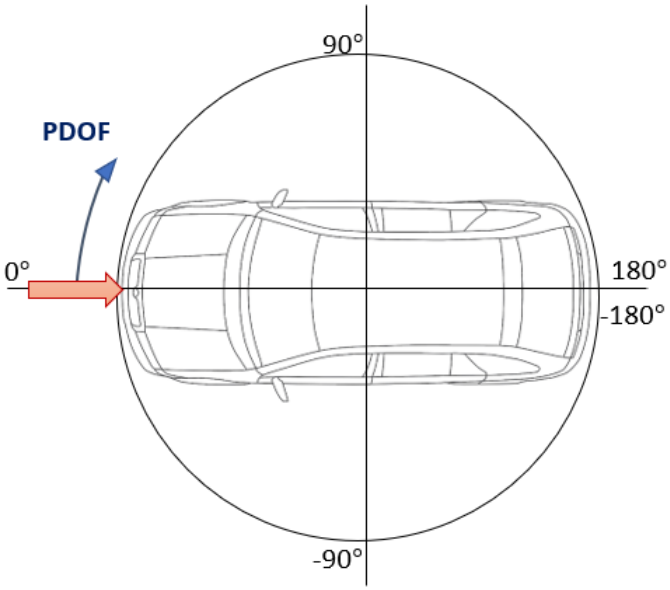

Figure 2.1: Illustration of PDOF and crash angle.

2.1.3 Abbreviated injury Scale (AIS)

The injury information provided from the databases is usually presented as the Abbreviated Injury Scale (AIS) code, proposed by the Association for the Advancement of Automotive Medicine (AAAM) [29]. The AIS scoring system classifies injuries based upon body regions and injury severity. The last digit in the AIS code denotes the severity of the injury on a six-point ordinal scale ranging from 1 (minor injury) to 6 (unavoidable death) as shown in Table 2.1 [30]. AIS had been updated over the years, with currently the most recent version being AIS-2015 [31].

Table 2.1: The AIS scoring system with injury severity classifications.

AIS code	Injury severity	AIS% prob. of death
1	Minor	0
2	Moderate	1-2
3	Serious	8-10
4	Severe	5-50
5	Critical	5-50
≥6	Unsurvivable	100

All the injuries in this study are considered at the AIS2+ level, according to AAAM 2005. In the case of concussion, AIS2+ denotes moderate concussion

severity. In the case of rib fractures, AIS2+ denotes an injury equivalent to having two or more fractured ribs [32]. When it comes to the lumbar spine injury, AIS2+ stands for minor and major compression lumbar injuries, with compression being the most common AIS2+ thoracolumbar spine fracture type [33].

2.1.4 Virtual FE reconstructions of real world MVCs

Having access to real world crash data through databases allows researchers to re-create an accident event in a virtual environment. Input data to the simulation might consist of occupant sitting position, safety restraint system conditions, friction values for the various surfaces, velocity and the impact angles etc [34].

Two different types of MVC reconstructions can be distinguished – population based MVC reconstructions and detailed crash reconstructions. Population reconstructions are relying on statistics and the injury is evaluated by comparing risk curves for both the real-life crashes and the stochastic reconstructions [14]. In contrast to population reconstructions, detailed MVC reconstructions are considering only a few real-life crash cases with a higher level of details.

2.2 Previous detailed crash reconstruction studies for HBM validation

FE detailed crash reconstruction is the validation method used in the present study and has previously been utilized in numerous other projects [35], [14], [36]. The data of the real crashes were in most studies obtained from CIREN or NASS-CDS databases. Two previous studies, [8] and [9] from Virginia Tech, were carried out based on the very same 11 MVC cases as in the present study. In [8], the lower extremity injuries were validated of a THUMS v4 with a simplified vehicle model (SVM) reconstructing eleven real-world motor vehicle crashes. In order to determine the injury risk of AIS 2+ lower extremity injuries, multiple functions were used such as femur force, tibia force and moment or tibia index.

Similar approach has been used also in study [9] in order to predict thoracolumbar spine fractures. A lumbar spine criterion was developed to account for combined effects of measured axial compression forces and bending moments in thoracolumbar vertebrae. The lumbar spine index without age scaling correctly

predicted 9 of the 11 cases, while the age-adjusted index was correctly predicted for 10 cases.

Furthermore, study [37] has used reconstruction of a real world near-side impact crash in order to predict thoracic, brain, abdominal, and pelvic injuries. Also, here the THUMS v4 and SVM was used to recreate a real-world vehicle accident. For the head injury assessment, head injury criterion (HIC) was implemented considering head acceleration. For the thorax, a thoracic trauma index (TTI) was calculated by the accelerations of three ribs. Also, spinal, and pelvic accelerations were measured. The simulation results correctly predicted the injuries of the thoracic, abdominal and pelvic, but not those of the head.

In study [11], SVM was tuned and used along with scaled THUMS occupant in LS-Dyna simulations to reconstruct one real world MVC case from CIREN. To predict sternum and rib fractures, tissue injury metric stress and strain were used. In addition, also chest deflection measurement and local forces and moments in the lumbar vertebrae were evaluated. Finally, obtained injury risks were compared to real-world injury outcome.

2.3 Head injury

Below follows a brief overview of head anatomy, head injury severity and Mechanism of Injury (MOI) description for increased understanding of the resulting injuries.

2.3.1 Head anatomy

The human head anatomy is very complex. Looking from outside to inside, the first to encounter is a 5-7 mm thick scalp, followed by skull bones which are protecting the brain from impact [32], see Figure 2.2. Thereafter follows multiple layers of the cranial meninges membranes, such as dura mater, which separate the brain from surrounding bones.

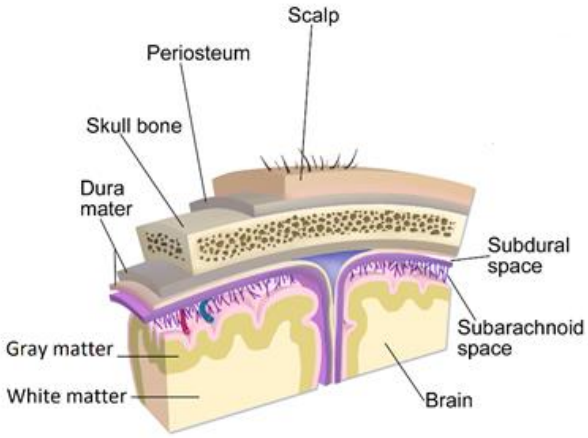

Figure 2.2: A cut-out illustration of layers covering the human head. Adopted and modified from Wikimedia, Medical gallery of Blausen, [38].

The human brain tissue is composed of white and gray matters and consists of four major parts: brain stem, cerebellum, diencephalon and cerebrum, with the cerebrum being the largest part of the brain [15], see Figure 2.3. The cerebrum consists of two hemispheres which are interconnected by the corpus callosum [15]. The corpus callosum is a very important part of the brain since is responsible for connecting the two cerebral hemispheres and through which communication between them is carried out [39]. It is about ten centimeters in length, consisting of around 300 million axons (fiber projections of nerve cells) connecting nuclei (a cluster of neurons) of the central nervous system [40].

Gray and white matter are found in the central nervous system. Gray matter is the outer most layer of the brain, made of neuronal cells (cells responsible for carrying electrical impulses) and dendrites, short extensions with the main function to communicate signals to cells. As one of the main components of the central nervous system, gray matter controls most essential functions of the mind [41]. White matter, which lies beneath the gray matter cortex, is comprised of millions of myelinated axon bundles which are essential for processing and high-speed transmission of nerve signals between the different regions of the brain [42], [41]. Damage to the white matter can be harmful for the motor and cognitive functions.

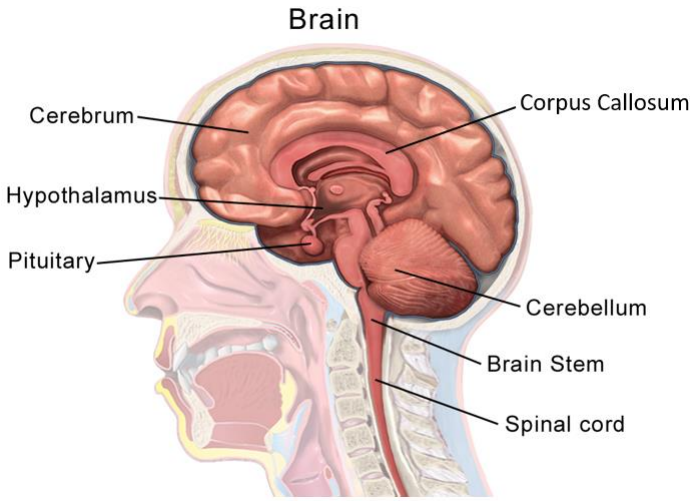

Figure 2.3: Cross-sectional view showing four major parts: brain stem, cerebellum, diencephalon and cerebrum. Adopted from Wikimedia, [43].

2.3.2 Head injury severity

Head injuries sustained by vehicle occupants, pedestrians, motorcyclists and cyclists are one of the most frequent and severe injuries in the European Union (EU) accounting for about the 40% of road fatalities [44].

Head injuries involve injuries to the scalp, skull and brain. Skull fractures and injuries sustained outside the cranium are classified as extracranial injuries [45]. On the other hand, there are intracranial injuries, commonly referred to as traumatic brain injury (TBI) caused by a sudden acceleration or deceleration within the cranium [45].

Focal and diffuse brain injuries are two clinically classified groups of TBI [15] [32]. Contusion and hematomas are typical focal brain injuries. Concussion and Diffuse Axonal Injury (DAI) are two typical diffuse brain injuries, common in vehicular accidents [46] [15].

Concussion, also called mild traumatic brain injury (mTBI), is the most common type of head injury [15]. It is caused by an impact into the head leading to brain quickly moving back and forth inside the cranium creating increasing amounts of acceleration-deceleration injury to the brain [46]. Although the mechanism behind the concussion and resulting symptoms are known, it is not clear in what way the brain is injured. However, a hypothesis is that concussion is a wide-spread injury in the brain volume.

Concussion symptoms are confusion, disorientation and varying degree of loss of consciousness [15]. Mild concussion causes temporarily unconsciousness, often for a few seconds up to couple of minutes [15]. More prolonged unconsciousness, when concussion continuous beyond six hours after the time of injury [46], is associated with DAI, leaving long term consequences [15]. Figure 2.4 shows a simplified head injury classification chart for a better overview of here mentioned injuries.

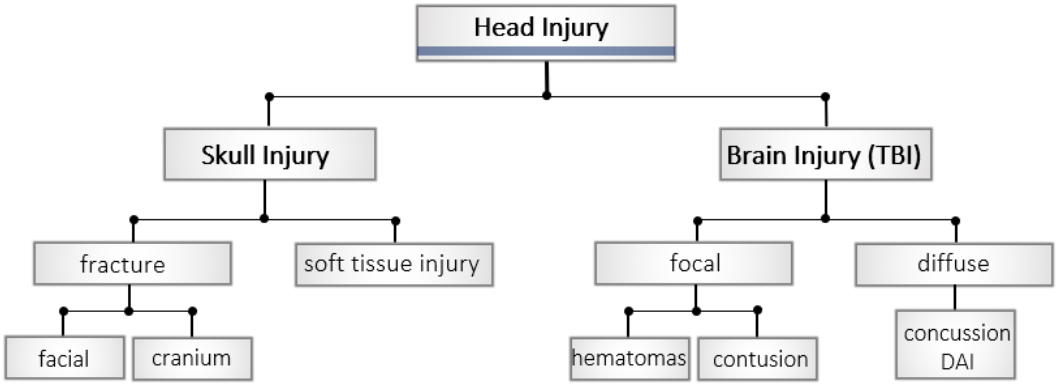

Figure 2.4: Head injury classification chart.

2.3.3 Head injury mechanism

The injuries of the brain and surrounding soft tissues can be caused due to impact of the head itself, the sudden movement of it or a combination of both [47]. In a vehicle collision accident, head impact duration is typically over within 200 milliseconds, which means that the resulting external mechanical loading is of dynamic nature. When the head is exposed to an impact like this, the generated mechanical energy is absorbed by the skull and further distributed throughout the brain. This non-contact loading caused by inertia puts the brain in motion, see Figure 2.5.

Figure 2.5: Illustration of brain movement as result of an impact onto the head. The image is retrieved from Wikimedia, [48].

2.3.4 Head injury criteria

Head injury criteria is commonly divided into global and local level criteria. Global level criteria is associated with head kinematics in form of translational and/or rotational accelerations of the head's Center of Gravity (COG) and local level criteria is considering stresses and strains in the brain tissue [49]. Currently the most widely used global criteria for head injury in automotive research is Head Injury Criterion (HIC) [32]. This criterion is used as a measure of the likelihood of head injury to arise from an impact, and is commonly applied for safety standards regarding head protection systems [2], [44]. However, HIC does not distinguish between different types of head injuries, such as skull fractures or DAI [44]. This makes the criterion irrelevant to use in case of a diffuse brain injury like concussion.

When it comes to local brain tissue injury measures for evaluating TBI, several metrics are proposed in the literature. In [2] (Kleiven, 2007), various predictors have been evaluated for concussion. [2] Study [2] is based on analysis of collected kinematics of concussive and sub-concussive impact data of 58 American football players from the National Football League (NFL). This set of data has been used as input along with the KTH Royal Institute of Technology head model, with the aim to compare various predictors for mTBI. The head model, with the skull treated as rigid, was subjected to linear and rotational acceleration pulses corresponding to kinematics data obtained from laboratory testing. It has been showed that there is a statistical correlation between concussion and several local

injury predictors: first principal strain, strain rate, strain energy density, product of strain rate and strain, maximum positive pressure, magnitude of minimum pressure as well as von Mises stress.

Although several different local injury metrics have been promoted in the literature, the first principal strain metric has been the most common choice as a predictor of DAI [2]. Hence, in the present study, the first principal strain metric is chosen for evaluation of concussion injury based on corpus callosum, gray matter and white matter. In [50] it was suggested that maximal principal strain higher than 0.18-0.21 (depending on the source) leads to DAI. Lower maximal principal strain values are according to study [51] instead representing a conservative threshold for concussion, with reversible injury to the axons.

2.4 Thorax injury

This section begins with a thorax anatomy description, followed by thorax injury severity, mechanism and criteria.

2.4.1 Thorax anatomy

The chest area, properly called thorax, is built of the thoracic wall consisting of the rib cage formed by twelve pairs of ribs, interconnected with three layers of intercostal muscles [52]. The thoracic wall encloses and protects the underlying soft tissue organs such as heart, lungs, trachea and large vessels. At the anterior ends (toward the front of the body), ribs are extended by costal cartilages bars which makes the thorax wall more elastic. The ribs are numbered 1–12 from the neck and down. The first seven ribs are directly attached to bony structure called sternum (breastbone) and are for this reason termed true ribs [32]. The lower ribs, eight to ten, are termed false ribs since they are indirectly connected to the sternum via the costal cartilages. The lowest two ribs are shorter than the rest and are known as floating ribs. Posteriorly (towards the back of the body), each rib is connected to a thoracic vertebra. Figure 2.6 shows a FE representation of the human ribcage included in the SAFER HBM.

The rib bones are made of two layers, namely cancellous (spongy) bone and compact bone [53]. Compact bone is a hard outer layer made up of living bone cells while the cancellous bone is the inner layer with cavities where the bone

marrow is housed. The characteristics of the bones depend both on sex (women's bones are usually lighter and smaller) and on the age of the person [53].

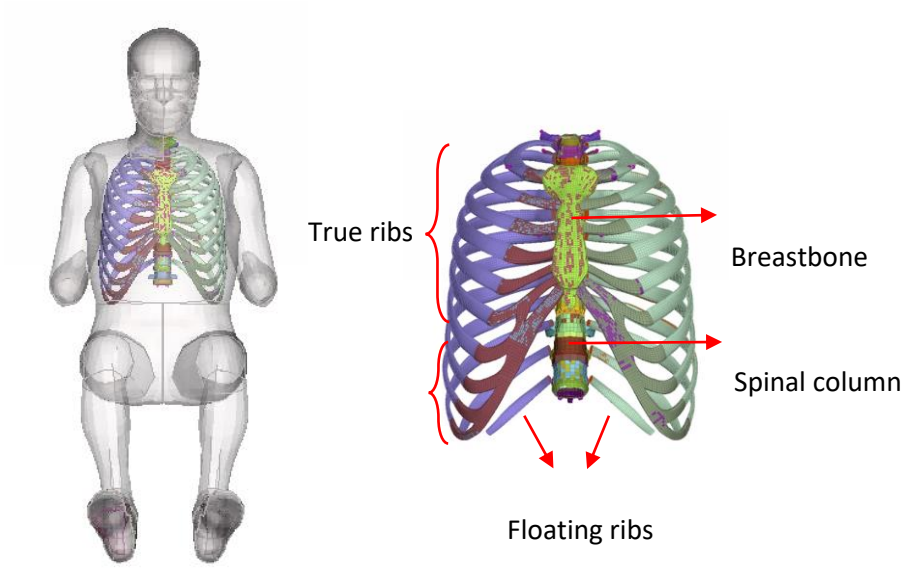

Figure 2.6: Ribcage in SAFER HBM v9.

2.4.2 Thorax injury severity

As one of the most injured body regions in vehicle collisions, thorax stands for approximately 30 % of fatal injuries in frontal collisions involving belted drivers over the age 34 [52]. Injury severity is increasing with increased number of fractured ribs (NFR). Single rib fractures (AIS 1) are mostly self-healing and generally pose no serious threat. However, with multiple rib fractures thorax wall may lose its overall stability which may lead to life threatening medical condition, especially among elderly [52] [32]. Analysing rib fractures provides a good indication of other thoracic and abdominal injuries [52].

2.4.3 Thorax injury mechanism

Rib fractures are highly influenced depending on the type of impact, the load exerted and the age of the person. In a vehicle crash, thorax is most commonly exposed to blunt contacts against interior of the vehicle.

During a rapid impact, such as in a vehicle collision, human anatomic structure is exposed to forces which are developed on the body due to the inertial resistance of tissues. The viscoelastic tissues of a human body are protecting vital organs

from undesired effects of certain impacts by absorbing energy [54]. However, forces acting upon the body that causes mechanical deformation of tissues beyond a certain failure limit results in damage causing an anatomic lesion or functional change. Commonly, ultimate strain is used as threshold at which material failure is expected to occur [8]. Although rib fracture can occur at any point, it is most likely for a fracture to occur at the point where an impact force is acting or at the point of maximum curvature, which makes lateral fractures more common due to the ribcage anatomy structure [32].

2.4.4 Thorax injury criteria

Human tolerance thresholds to impact are not straightforward to determine as tolerances depend on force characteristics such as its magnitude, direction and distribution [32]. Also shape and rigidity of the striking object are of importance. What makes it even more complicated is dependency of biological factors of individuals. For instance, the occurrence of rib fractures is strongly age dependent, as the ultimate strain of rib cortical bone has been shown to have a decreasing relationship with age [32].

When it comes to the thorax, injury criteria can be distinguished on three different levels: global, structural and material level [32], as illustrated in Figure 2.7. By means of global injury criteria level, injury mechanism is observed at the thoracic structure as a whole, such as chest compression. Structural injury criteria level is related to specific parts such as a single rib injury mechanism. Material injury criteria level is considering local behavior of a certain region, for instance stresses or strains in ribs.

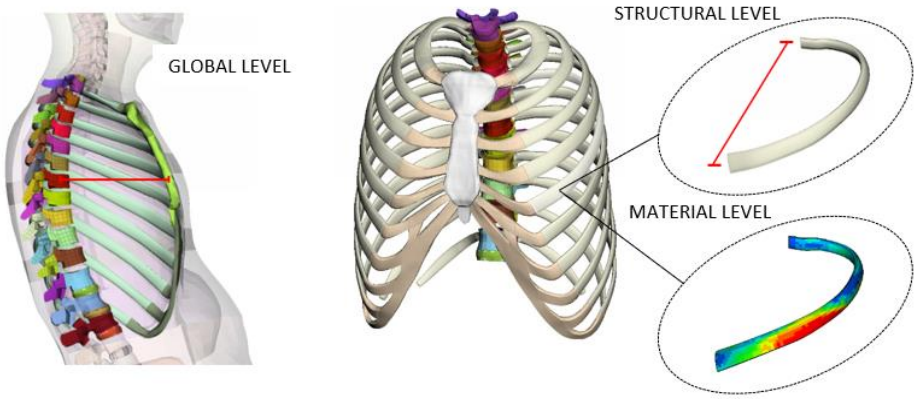

Figure 2.7: Illustration of injury measurements based on three different injury criteria levels: Global, structural and material level.

Until currently, very few studies have been focusing on rib strain validation. In study [3] the main focus was on rib strain validation of the newly developed generic FE ribcage of SAFER HBM, intendent for tissue-based injury evaluation. As such, the study represents an important initial phase in the validation process of strain-based rib fracture criteria for HBMs. Rib stiffness and rib strain where accurately predicted based exclusively on anterior-posterior bending [3].

Once the HBM is validated for strain, there exist two categories of strain-based methods that can be used to predict rib fractures using finite element HBMs, namely deterministic and probabilistic approach [52]. With deterministic approach it is possible to predict an exact number of rib fractures. Elements are modelled to be freely removed from ribs when the strain exceed a specified threshold thus the location with element-elimination represents then rib fracture. However, deterministic methods are not capable of predicting injury occurrence in a population with varying physical characteristic, but are rather limited to fractures based on a specific set of occupant characteristics [55] [52].

With probabilistic methods, injury prediction is based on obtained probability in a given scenario accounting for variations in occupant characteristics [52]. Study [52] has assessed strain-based probabilistic framework to predict rib fracture risk. This has been accomplished using a whole-body FE model THUMS, performing three different frontal collision simulations and comparing the results to cadaver sled tests. Firstly, local rib fracture probabilities where estimated based on an age-adjusted ultimate strain distribution that was developed from a literature dataset of 133 tests. As explained in [52], fracture sites can either be defined as whole individual ribs, predicting the number of ribs expected to fracture, or based on local areas ("hotspots") of peak strain within the ribs with ability to predict potential multiple fractures within individual ribs. In a second step, these local probabilities were combined to predict injury risk for a certain severity level within the whole ribcage. Results showed that predicted numbers of fractures were consistent in comparison to cadaver tests.

2.5 Lumbar spine injury

This section describes the spine anatomy, followed by spinal injury severity, mechanism and criteria.

2.5.1 Spine anatomy

The human spine, commonly referred to as vertebral column, consists of a series of vertebrae bones separated by intervertebral discs. The spine is divided into five regions characterized by different vertebral structures: 7 cervical (C1 to C7), 12 thoracic (T1 to T12) and 5 lumbar (L1 to L5) vertebrae, followed by sacrum and coccyx bones which consist of multiple fused vertebras [56]. See Figure 2.8.

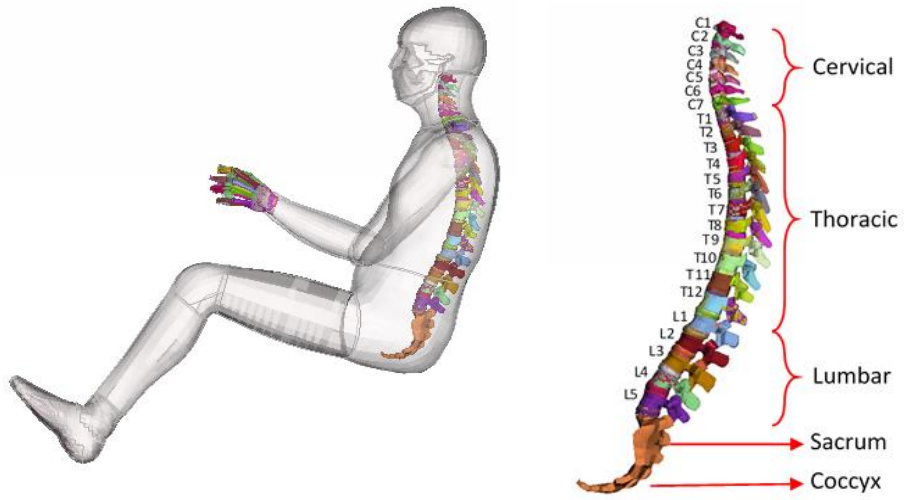

Figure 2.8: Vertebral column in SAFER HBM v9.

Each vertebra consists of a cylindrically shaped body followed by a vertebral arch. The lumbar vertebras are the largest segments of the vertebral column. Posterior of each vertebra, there is a bony projection called spinous process and on the right and left sides there are so called transverse processes which serve as attachment points for muscles and ligaments, see Figure 2.9. Vertebral column is protecting the spinal cord and supports the body weight above the pelvis, at the same time as it enables movement of the body [32].

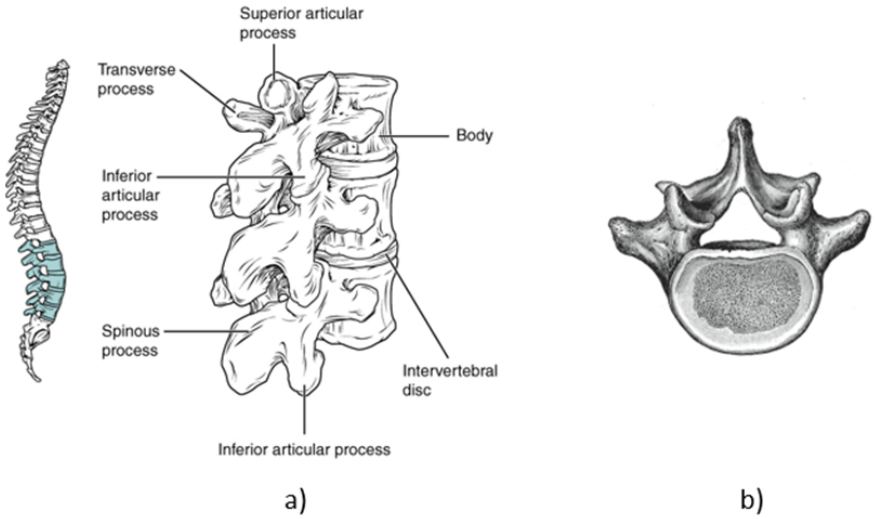

Figure 2.9: a) Side view of lumbar vertebrae adopted from Wikimedia [57] b) above view of a lumbar vertebrae adopted from Wikimedia, [58].

2.5.2 Spinal injury severity

MVCs are one of the main causing reason for spinal injuries [59]. In particular, study [33] has reported, based on real-world data gathered from Volvo Cars Traffic Accident Database, that spinal injuries are one of the top three most frequently injured body region in frontal crash accidents. In [32], it has been pointed out that the most frequent spine injuries in automotive crashes are at the most upper region of the vertebrae column, the cervical spine. Although, injuries to thoracolumbar spine (the thoracic and lumbar regions) are less frequent compared to cervical region, previous studies have shown that thoracic and lumbar spinal injuries have increased in relative importance [33], [60]. In fact, it has been shown, based on looking into the NASS-CDS database, that thoracolumbar fractures in frontal collisions increased in relation to vehicle model in the past decades [60]. Different severe injuries, such as burst, compression and dislocation fractures and anterior wedge fractures are possible to occur in thoracolumbar region, commonly resulting in low-back pain symptoms [33], [32].

2.5.3 Thoracolumbar injury mechanism

In the past decades, numerous experiments have been conducted on cadavers, with ATDs and even on volunteers restrained with a three-point belt in a vehicle collision [61], [62], [63], [64] etc. In this way the mechanical performance of the human spine was investigated [62]. It was generally acknowledged that the

thoracolumbar spine commonly suffers from wedge fractures on the vertebrae bodies through a generated compressive force. In study [65] it has been revealed that compression fracture were the most common fracture type when considering the whole spectra of accident situations, which also has been confirmed in study [33].

Spinal traumas can be categorized to minor and major injury based on spinal instability, according to Denis' system [66]. Minor injury involves transverse and spinous processes (see Figure 2.9) etc. Major spinal injury involves typically compression and burst fractures due to axial loading, but also fracture dislocation. Compression fracture affects anterior column (one-half of the vertebral body), and burst fracture affects both the anterior and middle column (entire vertebral body).

Along with the compressive force, also the bending moment appears to be the predominant injury loading type causing thoracolumbar fractures [9]. The most frequently injured vertebras in thoracolumbar spine are the ones located on the transition region between the thoracic and lumbar region [33] [65].

2.5.4 Thoracolumbar injury criteria and thresholds

Fracture threshold for the lumbar spine due to compression is through different experiments observed to occur around 2-6 kN [32]. Nevertheless, it is of importance to bear in mind that derived thresholds are restricted to a certain test conditions and thus dependent on a variety of factors such as various anatomical structures and impact directions [32].

Although some studies have been performed to investigate thoracolumbar response, there is yet no standardised injury criteria established for thoracolumbar fractures evaluation [9], [32], [67]. In contrast to cervical spine for which several neck criteria have been developed, the lack of injury criteria for thoracic and lumbar spine makes injury assessment more uncertain.

One recent attempt to develop a lumbar criterion has been made in study [9]. As previously pointed out, this study performed reconstruction of 11 motor vehicle crashes (the very same cases that are used in the present study), with six cases having thoracolumbar fractures. The study presented a newly developed injury criterion, called Lumbar Spine Index:

$$Lumbar\ Spine\ Index = \frac{F_z}{Fc} + \frac{M_r}{Mc} \tag{2.1}$$

where F_z stands for obtained axial compression force and M_r stands for the resultant bending moment of M_x and M_y (lateral bending moment and forward bending moment, respectively). Critical values, F_c and M_c, correspond to 90% of the average peak axial compression and resultant bending moment of all lumbar vertebrae. The obtained results from simulations showed that the criterion predicted thoracolumbar fracture occurrence for 9 out of the 11 cases. Also, age adjustment of the criteria was explored, which slightly improved the prediction. However, since the involved critical values are case dependent, this novel criterion is limited in its application in a more general manner.

3 Method

The method chapter describes how the SAFER HBM was positioned into the SVM using ANSA as an initial step to running the simulations in LS-DYNA. Also, post processing methods used for extracting the strains for rib fracture and concussion injury validation are described. Further, the method for extracting forces and moments in each lumbar vertebra for lumbar spine injury validation is described including chosen injury criterion and comparison to the injuries obtained from the databases.

3.1 Model setup

Before running the FE-simulations of reconstructions cases presented in Table 1.1, the model set-up was necessary. The approach for model setup involves check of units, positioning the SAFER HBM, seatbelt remodelling and defining contacts as described below. The initial and bounday conditions, such as accelaration pulse, were already predefined for each case based on the EDR, accounting only longitudinal crash pulse. Therore, the applied crash pulses are not a considered topic in the method section.

3.1.1 Model units

Simulation in LS-DYNA requires a consistent system of units to be used. In this case, units of the simulation model were predefined to a consisting system of units according to the units of the SVM: mm for length, seconds for time, tonne for mass, N for force, MPa for stress and N-mm for energy. In order for the simulation model to be compatible, the consistency of this system of units needs to be preserved. Since the SAFER HBM was defined in another system of units, it has been included with the *INCLUDE_TRANSFORM command, which matched the units of the SVM.

3.1.2 Positioning of the SAFER HBM

By mimicking the driver's posture in real-world crash cases, the chance to correctly predict injuries increases, hence, when positioning the SAFER HBM into the SVM, the goal was to obtain a posture as similar to the real occupant as

possible. The first step was to translate the HBM so that the midpoint of the hip (H-point) reached the desirable position. Once this was achieved, the SAFER HBM was rotated as an entire rigid body in order to obtain a proper sitting position, similar to the described posture of the real occupant.

Next, matching the position of the head, hands and legs was remaining to achieve a final posture. This was achieved using the Marionette method. This method is based on positioning cables which pull away the body part they are attached to. The positioning cables were modelled as one-dimensional element beams with a discrete element damper, see Figure 3.1

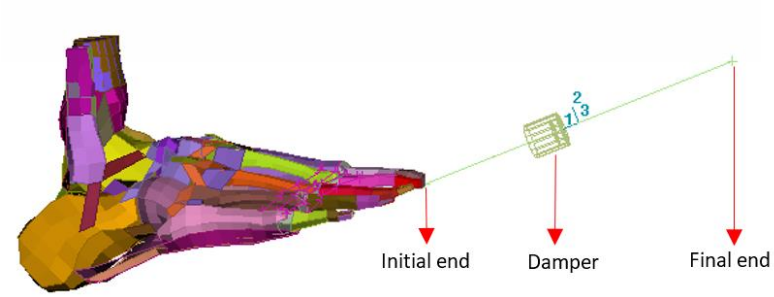

Figure 3.1: Example of a cable for positioning.

The initial end of a cable was attached on a node belonging to a bony structure part of the SAFER HBM. The another (final) end was fixed in space with the coordinates corresponding to the desired final position that the initial end of the cable is intended to reach. Pulling force from the cable corresponds to 0.5kN. To actually pull the cables and thus translate attached SAFER HBM body parts required running a simulation in LS-DYNA. This positing method have been applied to all of the 11 different reconstruction cases. Figure 3.2 shows an example of cable attachments in initial position and a final position after the cables have been pulled. One cable on each foot and each hand appeared to be sufficient to achieve a matching posture in most of the cases. For few of the cases, it was necessary to attach a cable also onto the head in order for it to be facing horizontally and also on the hips to make sure that the H-point of the SAFER HBM does not move. Appendix A show the final postures of the (unscaled) SAFER HBM for the 11 cases.

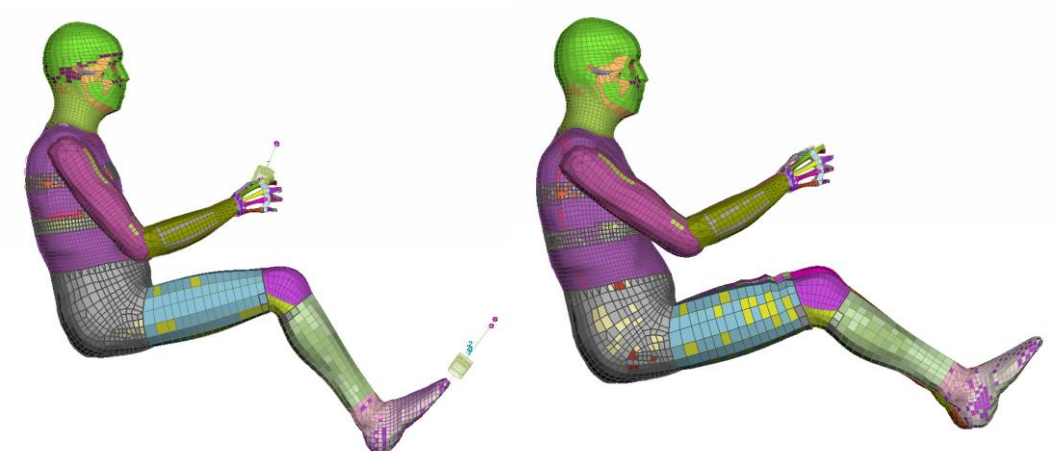

Figure 3.2: Positioning of the SAFER HBM with the marionette method.

3.1.3 SAFER HBM scaling

The SAFER HBM was scaled for cases 1-2 and 6-7. Case 1 and 2 had misaligned position of the head in vertical position because these occupants where only 165 cm (comparing to the 175 cm height of the SAFER HBM). Moreover, the driver seat for the case 6 and 7 had to be translated rearwards in order for the SAFER HBM to fit in without any penetrations to the instrumental panel. This cases where therefore scaled and an improved posture was obtained. The scaling was based on the expression from previous studies [8] and [9], where the THUMS v4 was volumetrically scaled according to following expressions:

$$Height\ factor = \frac{case\ occupant\ height}{SAFER\ HBM\ height} \quad (3.1)$$

$$Mass\ factor = \sqrt[3]{\frac{case\ occupant\ height}{SAFER\ HBM\ height}} \quad (3.2)$$

$$Volumetric\ scaling\ = \frac{Height\ factor\ + Mass\ factor}{2} \quad (3.3)$$

However, in the present study only case 6 has been volumetrically scaled where both mass and height factors where accounted. For the rest of the scaled cases, only height factor was used (so called isometric scaling). This choice has been based depending on which scaling method provided a closer match to the real occupant stature. The scaling was very easily implemented in ANSA with the

'Transform' tool such that the SAFER HBM was proportionally scaled in all directions (X, Y and Z) with the origin placed in the H-point.

3.1.4 Seat depenetration

Once the SAFER HBM is positioned in the driver seat, depenetration of the seat foam was carried out in ANSA. Depenetration deformed the cushion of the seat according to the SAFER HBM posture which is of importance for two reasons: 1) for taking into account the friction effects when SAFERM HBM glides onto the seat during the impact, and 2) to avoid possible contact penetration errors when running the simulation. Figure 3.3 shows an example of the depenetrated seat in comparison with the initial cushion form.

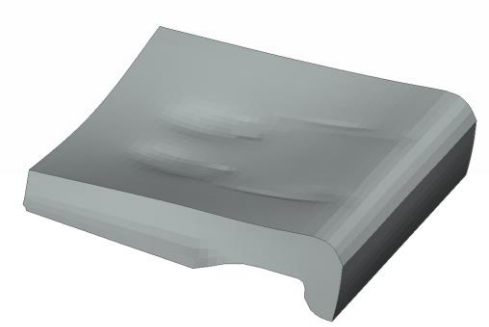

Figure 3.3: The seat depenetration due to the SAFER HBM posture.

3.1.5 Seat belt re-routing

The seatbelt was re-routed for each reconstruction case by using the seatbelt tool available in ANSA. Re-routing was performed by choosing a new interaction path of the lap and shoulder belt components. It was ensured that there were no improper contact interactions with the SAFER HBM that could cause a termination error when running a simulation. Other than this, all seat belt properties were kept unchanged from the original seatbelt model.

3.1.6 Contact definitions

The SVM consists of predefined contacts between its components, such as contacts between internal parts of the driver seat. Similarly, the SAFER HBM contains predefined contacts between its internal parts. These internal-type of contact definitions were kept unchanged. However, contacts defining interaction of the SAFER HBM with the environment (the seat, the feet pedals, the floor,

the instrumental panel, the airbag and the left side door) were updated. These contact definitions have been provided in the current project and have previously been used in an existing robustness check analysis with the SAFER HBM. All of the provided contacts were defined in ANSA as *CONTACT_AUTOMATIC_SURFACE_TO_SURFACE, choosing SAFER HBM as a master surface and the different vehicle components as slave surfaces with various static and dynamic coefficients of frictions. One exception was the contact definition between the seatbelt and the SAFER HBM which was adopted from the original model setup.

3.1.7 Running FE-simulations in LS-Dyna

After completing the set-up of the model, FE simulations were run on a cluster computer using LS-Dyna (R9.3.0) with single pression and Massively Parallel Processing (MPP). MPP allows LS-DYNA to run over a cluster of machines (a number of computers connected in a network). Each simulation run is ended after 180 ms. Analysing a crash during this time frame is sufficient in terms of injury validation. During this time frame, the HBM is exposed to a sudden forward acceleration, activating the restrain systems and colliding with the inflated airbag. Figure 3.4 shows an example of the collision for reconstruction case 1 at three different time frames. Visualisation of each simulation from the d3plot output file was done in META, in order to check that response behaviour of the model looks reasonable.

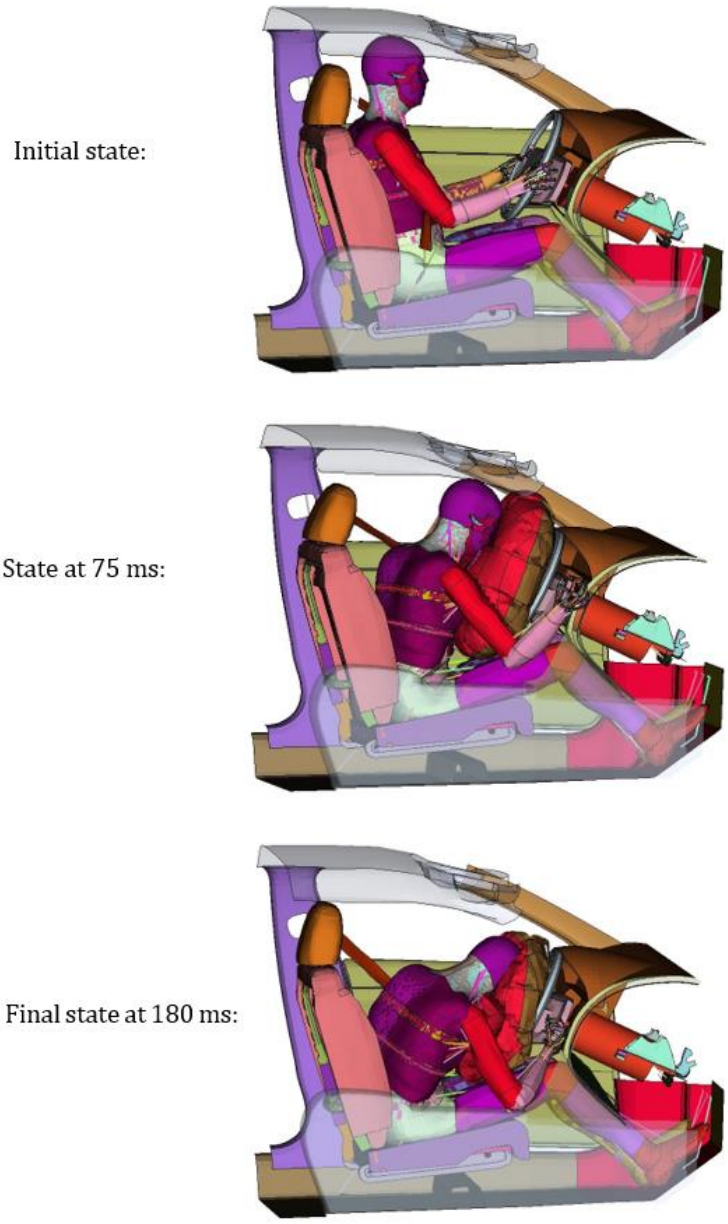

Figure 3.4: Impact at three different time frames (initial state, at 75 ms and a final state) for reconstruction case 1.

3.2 Estimating probability for concussion

The injury probability for concussion was estimated based on the 1st Principal Green St-Venant strain in the corpus callosum, gray matter and white matter, based on the findings in Kleiven, S. (2007) [2] where the same KTH brain model

was used for FE analysis of concussion. Figure 3.5 shows in red the ubication of the corpus callosum, gray matter and white matter in the head of the SAFER HBM.

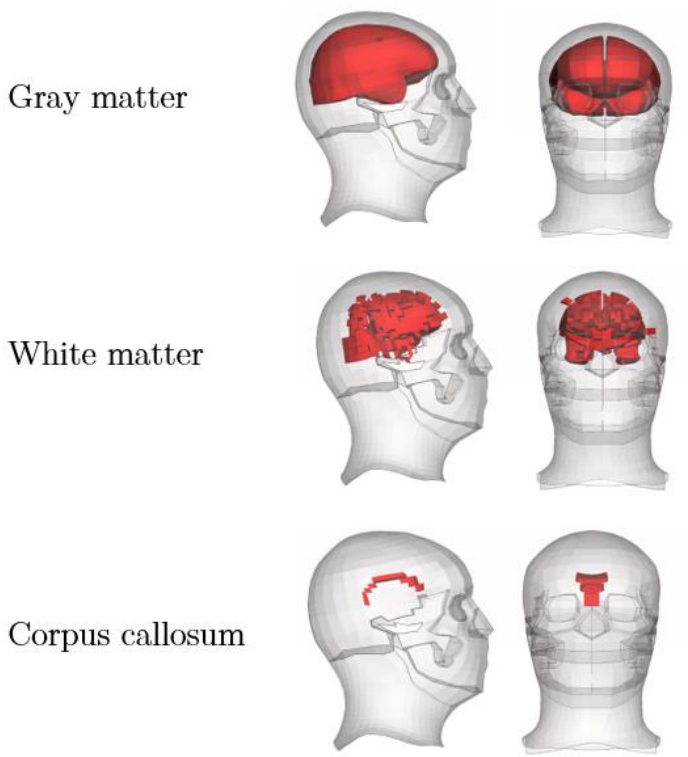

Figure 3.5: Analysed brain parts of the KTH brain inserted in the SAFER HBM.

The obtained strains in the brain of the HBM were analysed in LS-PrePost from a generated 3dplot output file. The 1st Principal Green St-Venant element strain was for each analysed brain part displayed for the sake of visualisation as a fringe plot, see Figure 3.6 for an example of this.

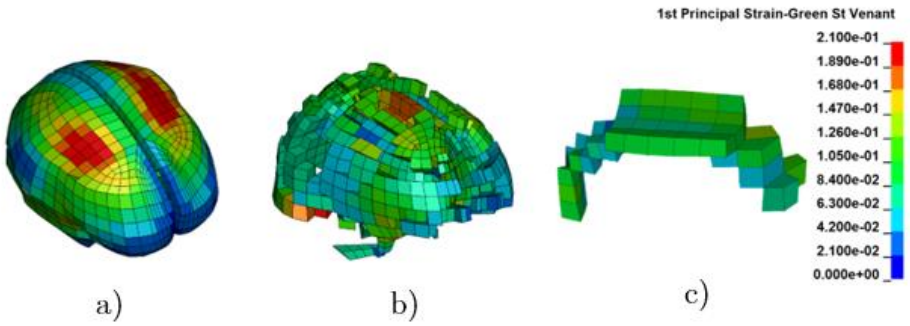

Figure 3.6: Strain distribution in a) gray matter, b) white matter and c) corpus callosum for case 1.

In the next step, the element time history strain plot was generated for each pertinent brain part. Figure 3.7 shows example of this in the case of corpus callosum and reconstruction case 1. As can be noticed, the plot indicates peak strain value and corresponding simulation time (state). 11 corresponding graphs were obtained per each brain part and per each reconstruction case.

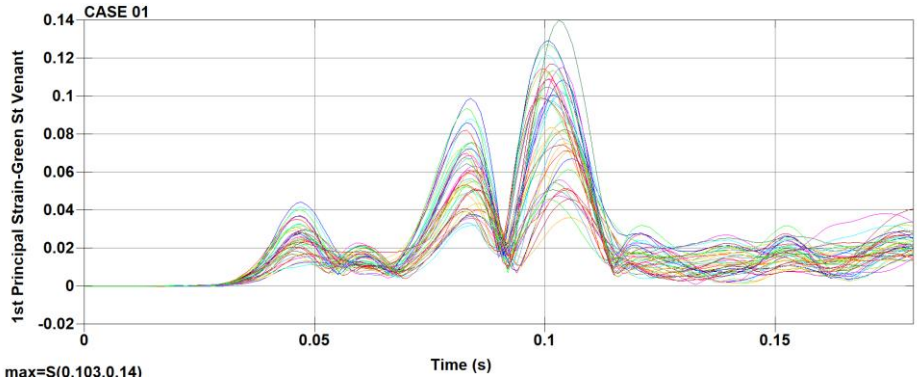

Figure 3.7: Example of a time history plot for case 1.

The maximum strain value was then used to find a corresponding ASI2+ probability value for concussion by looking into the logistic regression risk curves shown in Appendix B. These risk curves (one for each part of the brain that is studied) were created according to Kleiven, S. (2007)[2], but adapted for AIS2+ level injury by applying the equation (3.4) with changed parameters b0 and b1:

$$\mathrm{p} = \frac{1}{1 + e^{-(b0+b1\cdot X)}} \qquad (3.4)$$

where p is the probability of AIS2+ concussion and X is the predictor, in this case the measured 1st Principal Green St-Venant strain. The curve parameters $b0$ and $b1$ are depending on the brain part as shown in Table 3.1. The procedure to obtain the probability of AIS2+ concussion was the same for all the three tissues.

Table 3.1: Used parameters for plotting the risk curves for gray matter, white matter and corpus callosum, according to Kleiven (2007) [2].

Parameters	**Gray matter** (PID=44700101)	**White matter** (PID= 44700151)	**Corpus callosum** (PID=44700152)
b0	-4.1058	-4.1643	-3.5823
b1	9.0803	8.9442	10.1452

3.3 Estimating probability for rib fractures

Estimation of rib fracture AIS2+ probability is in this study based on local (tissue) criterion by considering maximum principal strain in the ribs. The procedure has been divided into two main steps: 1) extracting the peak value of maximum principal strains in each rib and 2) combining the extracted peak strain values into an AIS2+ probability fracture risk for the entire ribcage. This strain-based probabilistic method implemented here corresponds to what have previously been done in study [52].

In the step number one, a script (not included here) was implemented to extract the strain time histories for each rib in all of the reconstruction cases. The script was run in LS-PrePost, on a cluster computer where the crash simulation output files were located. In this way, the script generated one plot for each rib, showing time history of maximum principal strains in all of the elements of the corresponding rib. In total, 24 peak strain values were obtained in the plots for each reconstruction case. Figure 3.8 shows the maximum principle strain of the rib cage of case 1.

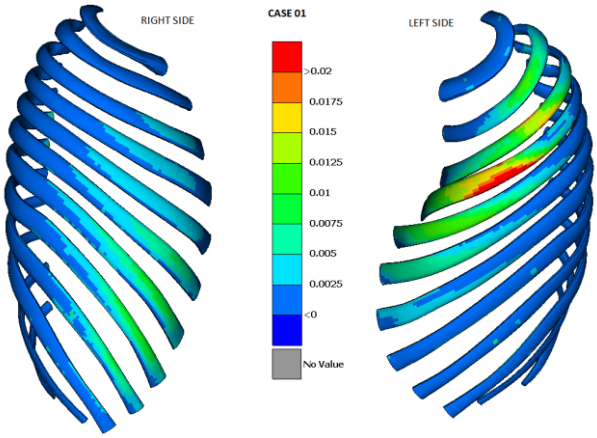

Figure 3.8: Illustration of max principle strain distribution in the ribcage of case 1.

As the second step, the 24 peak strain values from a reconstruction case were combined into an AIS2+ risk for the whole ribcage. This was established by implementing another script (AIS2p.R, see Appendix C) that was run in the statistical computing software "R". The computation algorithm of the R script was based on Poisson Binomial (PB) distribution including age adjustment. Underlying reason for using PB distribution is due to having varying fracture

probability for each of the 24 ribs. In study [68] PB distribution is described as: *"the probability distribution of the number of successes in independent but not necessarily identically distributed binary trials."* Expression for PB distribution can be formulated according to [68]:

$$\Pr(X = k) = \sum_{A \in F_k} \prod_{i \in A} p_i \prod_{j \in A^c} (1 - p_j) \quad (3.5)$$

where X stands for total number of fractures in the ribcage, p_i is for probability of fracture at the i^{th} rib number and F_k represents a set of all subsets of k integers that can be selected from $\{1,2,3,\ldots,n\}$ with n = 24 in this case. The script calculates AIS2+ risk by combining probability of fracture risk for individual ribs through PB distribution. The required input values to the R function are a file name, a vector with 24 elements for each peak strain value and the age of the occupant. In study [52], the authors have presented an Empirical Cumulative Density Function (ECDF) for rib material failure based on tensile testing. It was concluded that the rib ultimate strain decreased by 5.1% per decade. Instead of creating an ECDF in the implemented R script, a Weibull distribution was fitted to the strain data points, similar to study [69]. This provided a smooth risk function such that small increase in strain will give a small increase in risk for individual rib fracture with age adjusted distribution. Weibull distribution is for this case formulated as:

$$Rib\ failure\ risk(x) = 1 - e^{-\left(\frac{x}{\lambda}\right)^k} \quad (3.6)$$

where x is the strain, $k = 4.2495$ is the shape factor and the scale factor $\lambda = 36578.7 - 165.5 \cdot Age$. Eventually, the procedure involving steps 1) and 2) as described above was followed for all of the 11 reconstruction cases. The obtained probability values are summarized in Table 4.2 in the result chapter.

3.4 Lumbar spine injury assessment

Forces and moments are commonly used metrics for thoracolumbar spine injury assessment (as it has been pointed out in the literature overview). In particular, compression forces (F_z) and flexion moment (M_y) have been proposed to be major loads causing compressive vertebral body fractures. Below follows explanation of how this metrics have been extracted from the simulations and description of the criterion used for injury assessment.

3.4.1 Lumbar load cells

The SAFER HBM has initially been modelled with load cells using *DATABASE_CROSS_SECTION at each lumbar vertebra body. The load cells cross sections were located transversely through the center of gravity and were used to measure forces and moments in elements of the mid-vertebral cross section region. The loads in vertebra L1-L5 were measured in predefined local coordinate systems according to SAE J211, which were aligned to a corresponding vertebral cross section as shown in Figure 3.9. The local coordinate systems were located according to [70] with positive z-direction pointing downward and positive x-direction pointing forward. Following this sign convention means that tension forces in upper and lower lumbar spine occurs when chest is pushed upward and pelvis downward [70]. Similar approach for measuring lumbar loads have been implemented in studies [8] and [9] etc.

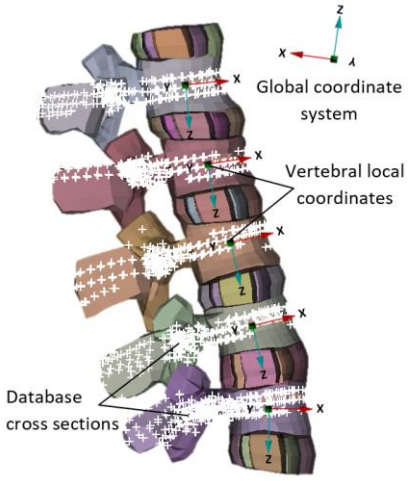

Figure 3.9: Lumbar spine with cross section database and local coordinate systems.

3.4.2 Lumbar spine injury index

In order to relate the measured loads to injury, a lumbar spine criterion was implemented, see equation (3.7). The criterion is termed $L_{index,C}$ where L stands for lumbar and C denotes compression force. The closer criterion value is to one, the larger probability it is for injury risk.

$$L_{index,C} = \frac{F_{z,compr}}{F_{z,crit}} + \frac{M_r}{M_{r,crit}} \ (< 1) \qquad (3.7)$$

The criterion combines the calculated compression force ($F_{z,compr}$) with the calculated resultant moment (M_r) - resultant of later bending moment (M_x) and flexion moment (M_y). $F_{z,compr}$ and M_r were extracted in the postprocessor META from generated binout run files. This criterion corresponds to the lumbar spine index (3.7) developed in study [9]. However, there are some major differences. In study [9], the critical compression force ($F_{z,crit}$) and critical resultant moment ($M_{r,crit}$) were decided based on the obtained simulation results from accident reconstructions. In order to make the criterion more generic, these threshold values, Fz,crit = 4.5 kN and Mr,crit = 180 Nm, were in this project chosed based on the results from isolated physical spine tests [71] and [72]. Authors in study [71] have experimentally quantified lumbar spine axial tolerance based on over 20 human lumbar spine specimens subjected to axial acceleration. In study [72], flexion response of several cadaveric lumbar spines was investigated by subjecting each spine segment to flexion loading in a custom designed spine testing machine. The threshold of 4.5 kN is based on a compressive force limit representing a 50% fracture risk. Thus, $L_{index,C}$ criterion only takes into consideration the compressive forces as axial loading. Tension forces are of less importance since only compression vertebra fracture is of interest to analyse (as one of the most common fracture type).

Figure 3.10 shows an example plot of the pertinent loads measured in vertebras L1-L5 for reconstruction case 1. The curve trend of the loads shown in Figure 3.10 is representative for the rest of the cases. From the compressive forces plot, it can be seen that initial tension is followed by compression and later tension again. The initial tension is rather small, and is most probably caused by the combination of pretensioner and leg motion until the feet pedals are reached.

Moreover, it can be seen that the peak values of compressive forces and resultant moments for different vertebras do not coincide at the same time. In study [9], the lumbar spine index was calculated based on peak load values independently of time. However, in the present study an assumption has been made that the maximum index value from a certain time in history should be considered as the most critical, in terms of compressive vertebra fracture.

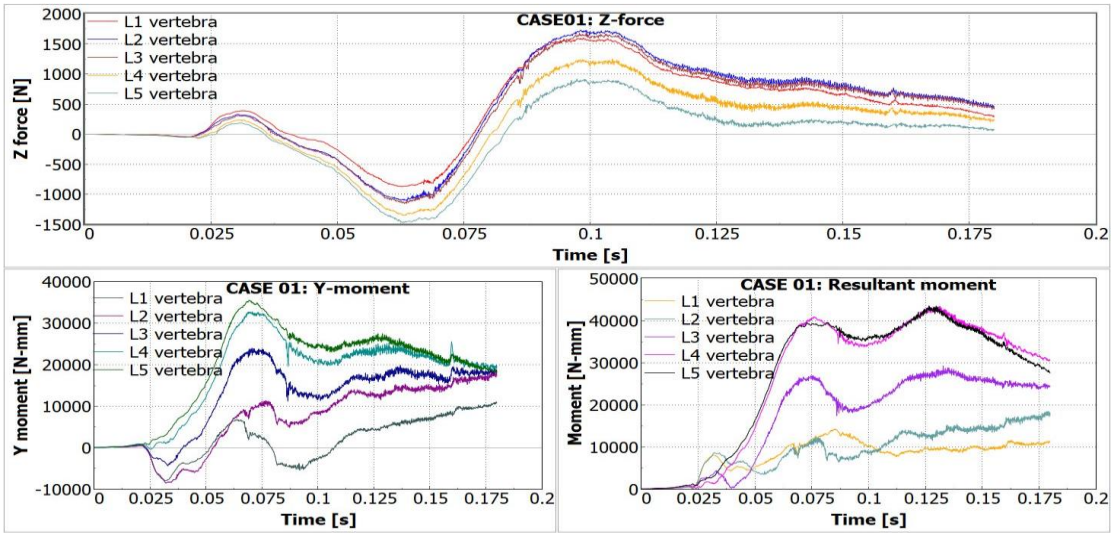

Figure 3.10: Example plots of measured F_z, M_y and M_r in vertebras L1-L5 for case 1, with time history from 0 to 180 ms.

4 Results

The chest and head (local) tissue criteria results and lumbar spine injuries results for the 11 reconstructed car crashes are summarized in this chapter. Only cases with the nominal height SAFER HBM have been presented in the below tables and diagrams. However, the comparison to the scaled models is summarized lastly in Table 4.4.

4.1 Concussion assessment

Extracted peak (1st Principal Green St Venant) strains in corpus callosum, gray matter and white matter for 11 reconstructed cases are presented in Figure 4.1. The highest strain is found in case 2 for which, according to the databases, no head injuries were reported and case 5, in which only minor head injuries were reported. The lowest strains are found in case 9 which is the case were unconcussioness (one of the most common symptoms of concussion) is confirmed in the databases.

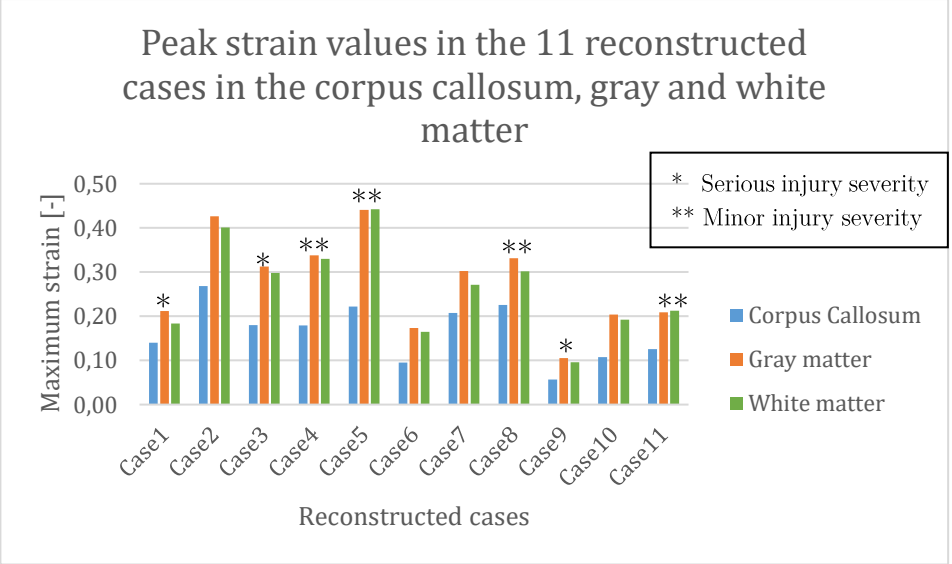

Figure 4.1: Maximum strain values in the corpus callosum, gray matter and white matter in the 11 reconstructed cases compared with the cases extracted from the databases which sustained any kind of serious (*) or minor injury severity (**).

The reported head injuries from the databases, and the probability of getting AIS2+ concussion injury based on the obtained strains from Figure 4.1 above, are summarized in Table 4.1. When comparing to the real-world injury outcomes, the probability is rather low in the cases 1, 3 and 9 where concussion is expected due to the severe head injury type. The probability range of these 3 cases is 3.5 – 22 %. For the rest of the cases, no sign of concussion is reported nor being expected and the obtained probability for the majority of the corresponding cases is below 50 %. Case 2 with the maximum probability of 44.1 % and case 5 with the maximum probability of 47.4 % are standing out with rather high probability between the cases for which no signs of concussion where reported.

Table 4.1: Reported head injuries of the 11 cases, and the obtained AIS2+ risk for concussion based on strain in the Corpus Callosum, gray matter and white matter.

		AIS2+ risk (%) based on strain		
Case Nr	**Reported head injuries (from databases)**	**Corpus Callosum**	**Gray matter**	**White matter**
Case 1	Subdural hematoma <0.6cm thick * Face hematoma Contusion of eyelids and periocular area (right eyelid)	10.3	10.1	7.4
Case 2		29.7	44.1	35.9
Case 3	Cerebrum contusion (<1cm diameter) *	14.7	22.0	18.3
Case 4	Facial Skin abrasion	14.6	26.2	22.9
Case 5	Facial skin abrasion Scalp abrasion	20.9	47.4	44.8
Case 6		6.8	7.4	6.4
Case 7		18.6	20.4	14.9
Case 8	Nose, mucosa/vessels rupture (epistaxis). Injury to the head NFS[1]	21.5	25.0	18.8
Case 9	Unconscious for <1h *	4.7	4.1	3.5
Case 10		7.7	9.5	8.0
Case 11	Skin/subcutaneous/muscle, face, laceration, minor, superficial (inferior/lower lips)	9.1	9.9	9.4

* (asterisk) indicates the cases with reported concussion and severe head injury.
NFS – not further specified.

Moreover, when making a comparison between the brain parts, it can be seen that the highest probability risk is obtained for gray matter in all of the cases except for case 1 and case 9. The largest probability deviation between all three

analysed brain parts when comparing within each case is 26.5 % (see case 5). In contrast, the smallest corresponding deviation is 0.8 % for case 11.

4.2 Estimated rib fractures probability

The maximum principal strain range in the ribs for the eleven reconstructed cases is 2.2-3.7 % with the largest peak values appearing in cases 2, 3 and 7, and smallest peak strain appearing in case 9.

Additionally, when analysing strains individually for each rib per each case, it can be seen that the largest strain occurs in the fourth left rib (L4), for all of the cases except for case 5 where the maximum strain is found in the third right rib (R3) instead. The reason for this maximum strain consistency in L4 is the interaction of the shoulder belt towards the chest. Figure 4.2 shows an example of the strain distribution in each rib of the case 1.

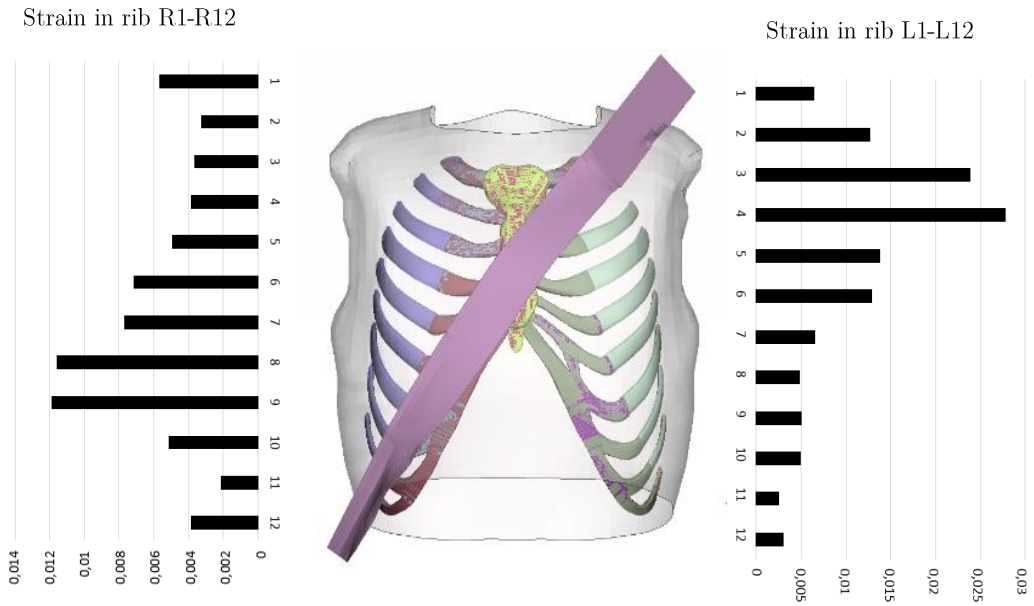

Figure 4.2: Strain distribution in the ribs for the reconstructed case 1. The distribution is representative for the rest of the cases, except for the case 5.

Table 4.2 summarizes the reported chest injuries from the databases, along with the probability of getting AIS2+ thoracic injuries of the reconstructed cases. The real-world multiple rib fractures have been reported for cases 6, 10 and 11. For

case 10, the estimated probability is 89.4 %. However, for case 6 and 11 the estimated probability is only 28.5 % and 41.7 %, respectively. For the rest of the cases with non-fractured ribs, the probability is rather high with a range of 32.6 - 94.3 %, with the highest probability assigned to case 2.

Table 4.2: Reported chest injuries from the databases of the 11 cases, and the estimated probability of AIS2+ risk rib fracture injury.

Case Nr	Age	Reported chest injuries	AIS2+ probability (%)
Case 1	67		52.1
Case 2	57		94.3
Case 3	43		59.0
Case 4	69	Sternum fracture Minor heart contusion	32.6
Case 5	23		38.6
Case 6	50	Bilateral 3rd rib fracture* Sternum fracture	28.5
Case 7	21	Hemomediastinum	42.8
Case 8	18	Pneumothorax	32.6
Case 9	80	Left Pneumothorax Lung Contusion	39.5
Case 10	86	Rib Fracture (L3-4, R 5-7,10) * Right Hemothorax; Sternum Fracture	89.4
Case 11	50	Rib Fracture (R 3-9) * Bilateral Pulmonary Contusion Sternum Fracture	41.7

* (asterisk) indicates the cases with reported multiple rib fractures (AIS2+ risk)

4.3 Estimated lumbar spine fractures

Selected cases for reconstructions involve six occupants with reported lumbar spine fractures according to Table 4.3. Table 4.3 also presents calculated $L_{index,C}$ for each vertebra for all of the cases. It can be noticed that five occupants in the real-world accidents sustained fractures at levels L1-L3, which are according to obtained $L_{index,C}$ estimated to have lower fracture risk than L4-L5 levels.

Table 4.3: Reported thoracolumbar vertebral fracture injuries in CIREN/NASS-CDS in comparison with obtained $L_{index,C}$ values for lumbar vertebras.

Case Nr	Vertebrae fractures (CIREN/NASS-CDS)	$L_{index,C}$ L1	L2	L3	L4	L5	Max($L_{index,c}$)
Case 1	-	0.248	0.290	0.381	0.498	0.529	0.529
Case 2	L4	0.225	0.258	0.414	0.562	0.595	0.595
Case 3	-	0.140	0.112	0.127	0.280	0.360	0.360
Case 4	L1, L2	0.265	0.311	0.376	0.540	0.628	0.628
Case 5	T12, L1	0.242	0.359	0.404	0.619	0.736	0.736
Case 6	T1-T6, T8, L1, L2	0.265	0.285	0.361	0.500	0.553	0.553
Case 7	-	0.306	0.378	0.459	0.612	0.689	0.689
Case 8	-	0.245	0.197	0.312	0.432	0.438	0.438
Case 9	L1, L3	0.157	0.162	0.257	0.391	0.429	0.429
Case 10	L3	0.131	0.149	0.247	0.365	0.394	0.394
Case 11	-	0.133	0.121	0.195	0.328	0.389	0.389

Values for $L_{index,C}$ is also presented in Figure 4.3, for better overlook of the data. From this plot, it is clear that $L_{index,C}$ progressively increases from vertebra L1 to L5, regardless of fracture outcome. When comparing the highest $L_{index,C}$ value for each vertebra level, it can be seen that the maximum levels for L1-L3 are seen in case 7 and for L4-L5 in case 5.

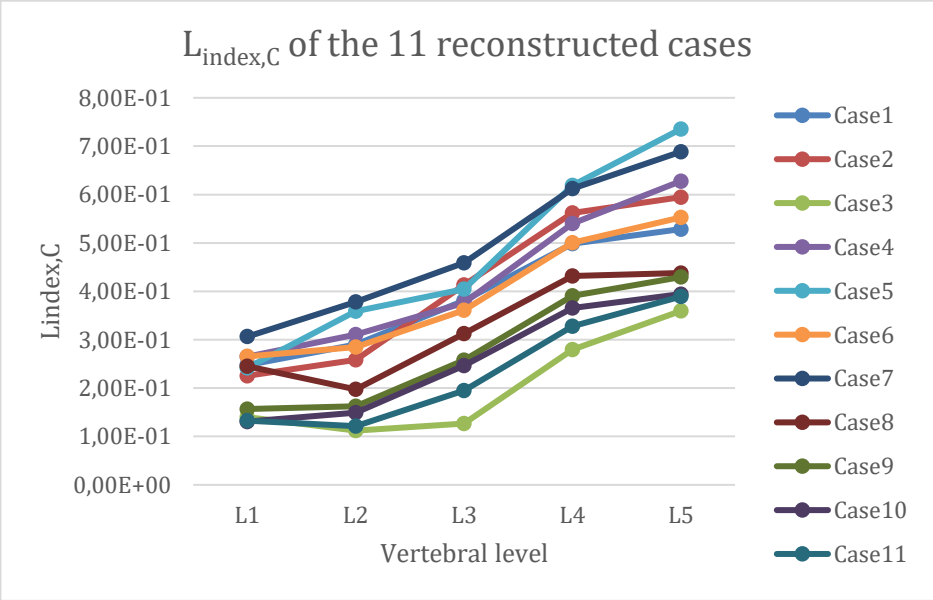

Figure 4.3: $L_{index,C}$ values of 11 reconstructed cases, categorized by vertebral levels.

The $L_{index,C}$ depends on the lumbar compression force ($F_{z,compr}$) and the resultant of lateral bending moment (M_x) and flexion moment (M_y). Figure 4.4, Figure 4.5

and Figure 4.6 present data individually for $F_{z,compr}$, M_y and M_r. On average, the occupants that sustained lumbar fractures have higher compression forces (L1-L5 $Avg\ F_{z,compr}$ = 1086 N) in comparison to the cases where occupants did not sustained any lumbar spine fractures (L1-L5 $Avg\ F_{z,compr}$ = 922 N). When comparing $F_{z,compr}$ for each vertebra level, it can be noticed that majority of cases with lumbar fractures have relatively high compression forces. Two exceptions are case 9 (L1) and case 10 (L3) which rather sustain an average compression force.

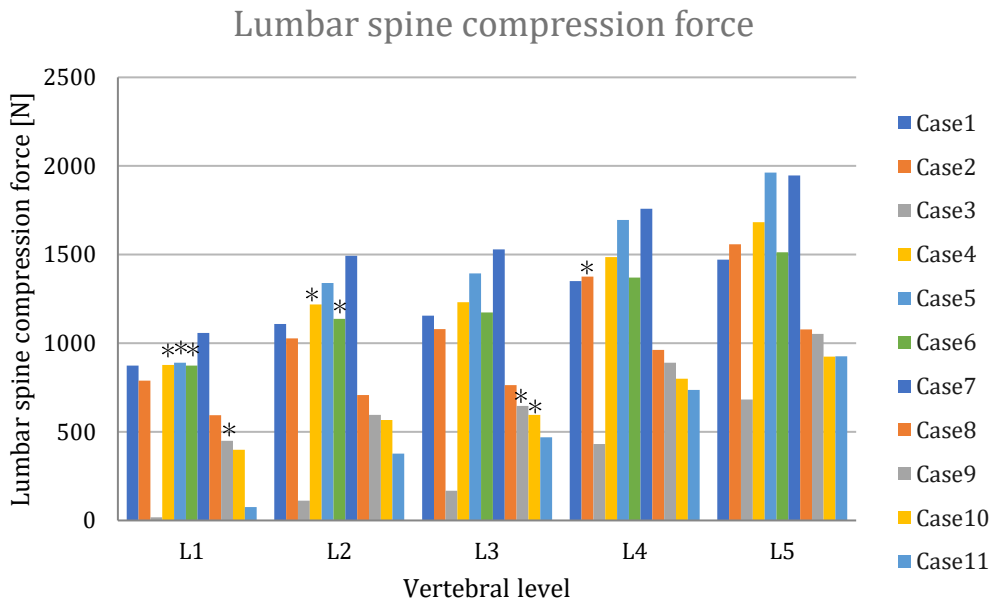

Figure 4.4: Measured lumbar spine compression forces (F_z) of the 11 reconstructed cases, categotised by vertebral levels. Asterisks indicate lumbar spine fractures according to the databases.

In contrast to the $Avg\ F_{z,compr}$, the average (L1-L5) flexion moment $Avg\ M_y$ for the cases that sustained lumbar fractures is almost identical to the average flexion moment of the non-fracture cases. When comparing M_y for each vertebra level, it can be noticed that only three of the cases (2, 9 and 10) with reported lumbar fractures have relatively high compression forces.

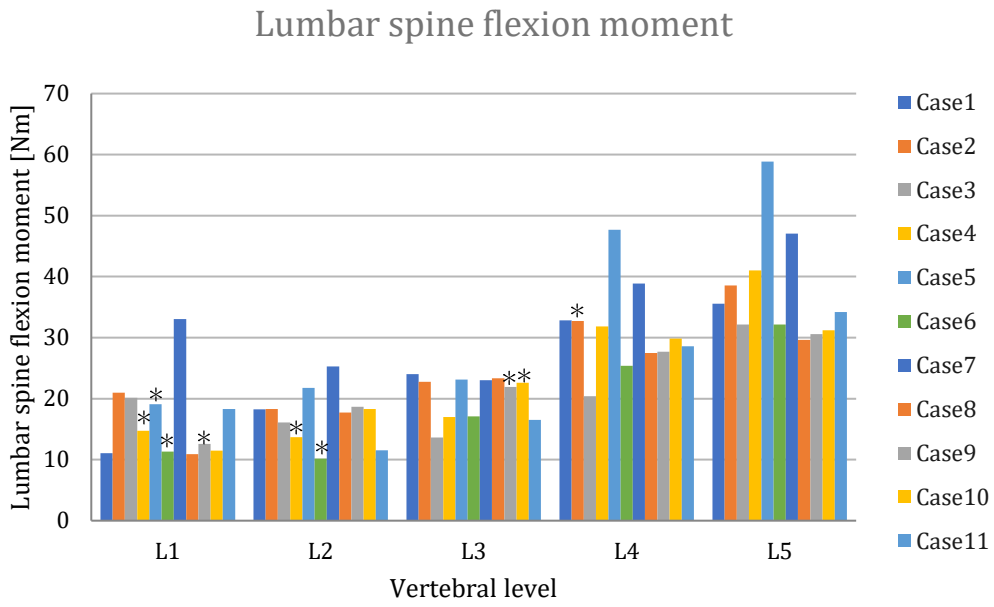

Figure 4.5: Measured lumbar spine flexion moments (My) of the 11 reconstructed cases, categotised by vertebral levels. Asterisks indicate lumbar spine fractures according to the databases.

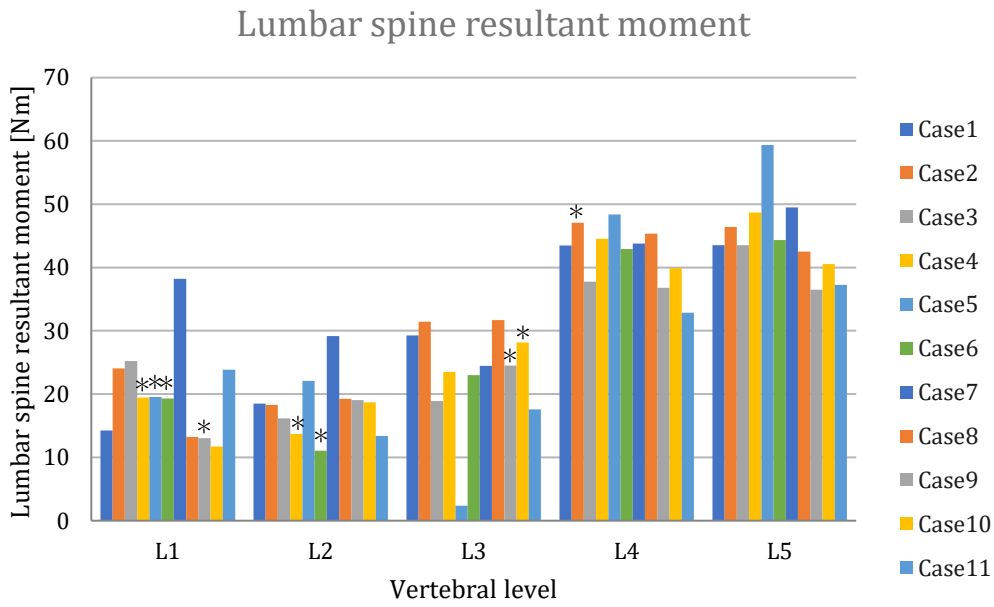

Figure 4.6: Measured lumbar spine resultant moments (Mr) of the 11 reconstructed cases, categotised by vertebral levels. Asterisks indicate lumbar spine fractures according to the databases.

4.4 Result comparison to scaled cases

In four of the cases, the SAFER HBM were scaled to determine if the scaled cases predict more accurate injuries than the unscaled cases. Lumbar spine injury validation is not obtained for scaled cases, since the lumbar spine injury criterion is based on averaged males, so that the critical compression force ($F_{z,crit}$) and critical resultant moment ($M_{r,crit}$) would most probably change when changing the size of the occupant, since the size of the vertebrae will also change.

However, the criterion used to determine head and rib injuries are based on strain, which in contrary to forces and moments in the vertebrae is insensitive to the scale of the model. Thus, the criteria used to determine head and rib injuries will continue to be valid for scaled cases. Table 4.4 summarizes the results obtained of getting probability of AIS2+ concussion for the corpus callosum, gray matter and white matter and the probability of AIS2+ rib fracture for the scaled and unscaled cases. It can be seen that fairly small deviations are occurring between the scaled and unscaled cases for all the analaysed brain parts and the ribcage.

Table 4.4: Comparison of the probability for scaled cases, including risk estimation for corpus callosum, gray matter, white matter and ribcage.

Case Nr.	Concussion AIS2+ prob. (%)						Ribcage AIS2+ prob. (%)	
	Corpus Callosum		Gray matter		White matter			
	Scaled	Unscaled	Scaled	Unscaled	Scaled	Unscaled	Scaled	Unscaled
Case 1	8.5	10.3	9.5	10.1	7.1	7.4	55.9	52.1
Case 2	33.6	29.7	41.1	44.1	31.2	35.9	84.1	94.3
Case 6	6.6	6.8	6.3	7.4	5.3	6.4	10.0	28.5
Case 7	15.2	18.6	18.5	20.4	13.7	14.9	38.8	42.8

5 Discussion

The discussion involves assessment of the obtained results and possible factors that might have influenced the outcomes. Discussion is further based on the measured metrics and the corresponding injury probabilities in relation to the real-world injuries reported in CIREN and NASS-CDS databases.

5.1 Influence of the SVM and crash case selections

It should be kept in mind that there is a certain risk for the SVM and the incorporated safety system not to be matching the physical vehicle. Each vehicle brand is highly optimized along with tuned safety system. Although the SVM has been tuned to represent different vehicle types from each reconstruction case, it is hard to match the actual properties of the vehicle in its entirety. This means that the safety systems might not work optimally together which could in overall affect results of estimated injury risks.

Moreover, the seat model in particular is most likely not a good representation of all the different seats in the reconstruction cases. In study [9] etc, it has been pointed out that the seatback angle had a considerable effect on the acting loads developed in the lumbar vertebral bodies.

What is in addition of importance to address is that the case selections where made with intention to include a broad range of common AIS 2+ rib and thoracolumbar fractures, and AIS1+ head injuries. In other words, all selected cases had representative injuries. This means that the 11 reconstructed cases are by no means a random sample of all occupants and crashes. The fact that occupants were injured and admitted to a trauma hospital can lead to speculation that the occupants represent a lower injury threshold (due to more fragile occupants) compared to the average population. The SAFER HBM and the corresponding injury risk estimates are meant to represent the average response of the whole population. In order for the sample of the cases to represent the average population it would be desirable to include cases with having a balance between uninjured and injured occupants.

5.2 Validation of the SAFER HBM posture

The height and weight of the SAFER HBM is not the perfect representation of all the occupants. Due to the differences in size between the real occupants and the unscaled SAFER HBM, it was not possible to match the posture perfectly well in all of the cases. Positioning hands onto the steering wheel, in combination with having a certain chest alignment was resulting in the constrained positioning of the elbows. However, this is expected not to have any significant effect on the result outcome of the pertinent injury predictions. More importantly was that H-point of the SAFER HBM was located in the correct position. Moreover, it was verified that the feet are positioned in the similar way as the occupant, close to the pedals and with no penetration to the environment.

Comparing the results from the scaled and unscaled cases, the differences are rather small for concussion and rib fracture evaluations. For the lumbar spine, the scaled model results were not considered, as it has been explained previously. Considering all this, it can be concluded that smaller deviations in the posture might result in small deviations in the results but that a perfect posture match to the real occupant is not necessary. The posture of the cases is therefore assumed not to have affected the final results in any significant manner. Nevertheless, it should be kept in mind that with morphed models, this influence might be of bigger concern.

5.3 Risk estimates - concussion

As it can be seen from the database injury description in Table 4.1, case 9 is the only case which has been reported to have suffered from unconcussioness, a strong indicator of concussion. However, subdural hematoma and cerebrum contusion have been reported for case 1 and 3, respectively. Although it has not explicitly been stated that occupants suffered from concussion, these injuries are assumed to arise the risk of sustaining it (i.e. leading to stretching of brain tissues which is one underlaying injury mechanism of concussion). Thus, case 1, 3 and 9 were expected to have much higher (over 50 %) estimated probability risk. For the rest of the cases that according to the databases did not suffer serious injuries, the obtained probabilities are not exceeding 47.4% (case 5), see Figure 5.1.

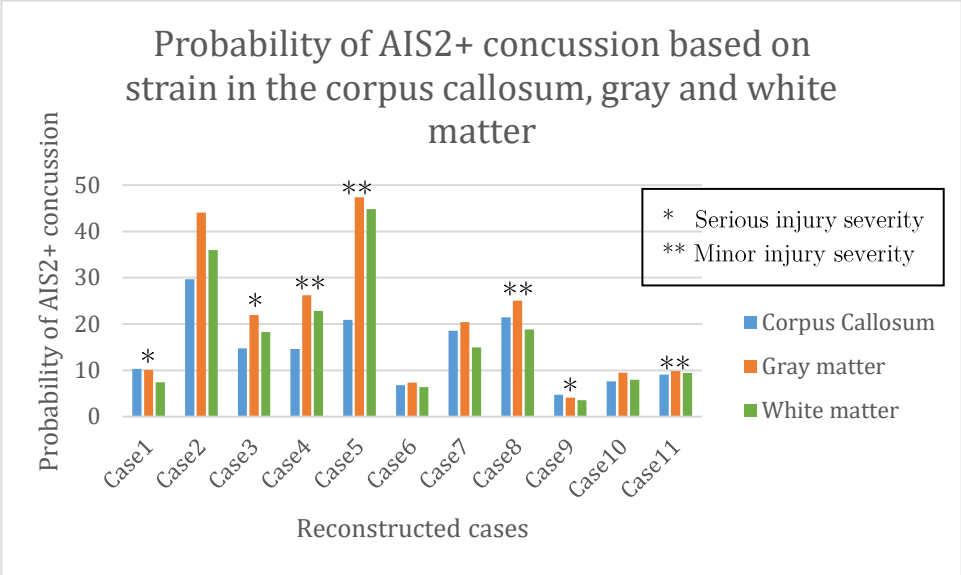

Figure 5.1: Probability of getting AIS2+ concussion in the 11 reconstructed cases, compared with the cases extracted from the databases which sustained any kind of serious (*) or minor injury severity (**)

When considering the overall results, average probability of getting AIS2+ concussion in this population of occupants is in the corpus callosum 14 %, 21 % for gray matter and 17 % for white matter. This can be related to the real-world outcomes, if considering that 3 out 11 cases (27 %) are concussion related cases. In other words, for the 11 occupants we could then expect 0.14·11 = 1.5, 0.21·11 = 2.3, and 0.17·11 = 1.9 occupants to be injured. This shows that all three brain parts underestimate the concussion risk in terms of average probability. However, the average probability should not be considered on its own (it rather serves as a complement to overlook the estimation).

The reason for not seeing desirable correlation of the concussion estimation in those cases that sustained serious injuries, might not only depend on the model characteristics, but rather on the applied method. It is of importance to emphasize that reconstruction simulations commonly involve uncertainties due to deviations from the real-world accident conditions. The overall outcome might be affected by many different factors, such as sitting positioning of the occupant prior to collision, belt placement, seat position, friction factors for the various surfaces, driver manuvers and the impact angles etc. More importantly, although the HBM might be positioned in the desired baseline posture, the initial head motion is not as well controlled as thorax for example. In order to minimise the ambiguity, it is desirable to have a more controlled head kinematics during the simulation. In

[2], the results of concussion estimations have been based on well documented head kinematics from real-world accidents observed through video recordings (observing NFL players). In addition, the initial head kinematics of laboratory testing has been reapplied in a simulation as input to the FE model [2]. In this way, it was ensured that head striking into a colliding object is alike the actual accident impact.

Another aspect that is worth noticing is that maximum strains for different cases and different brain parts appeared at different simulation time, distributed over simulation time 57-161 ms (minimum and maximum state range when accounting all the cases and analysed brain parts). Deviation in time for peak strains in different cases was to be expected due to the differences in the posture, but also varying deltaV. As it was pointed out in the literature overview, the mTBI can occur both due to the contact-impact and non-contact due to inertia effects. Interestingly, the time deviation for peak strain is also observed when comparing the brain parts of the same cases. This deviation was obvious for cases 3, 6 and 11, see Figure 5.2. For the rest of the cases the peak strain occurs more or less at the same states, which intuitively makes most sense.

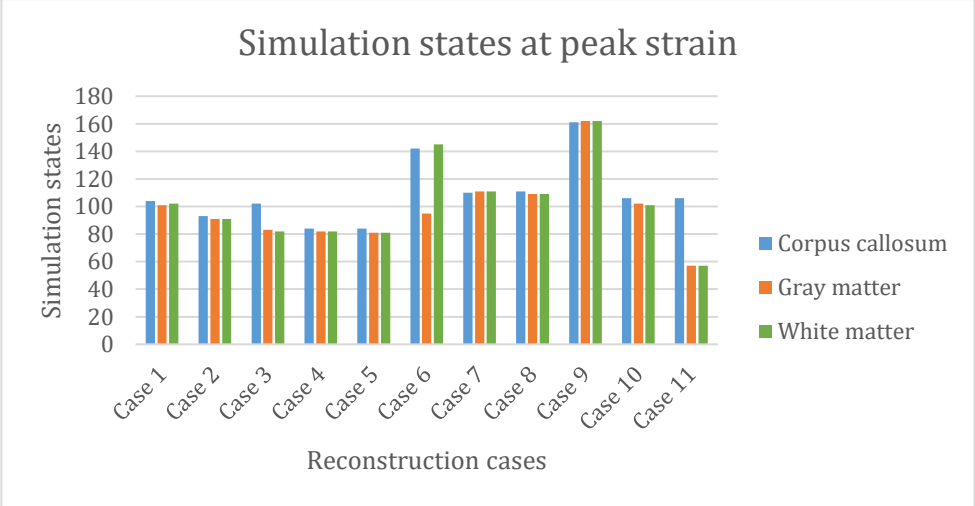

Figure 5.2: Comparison of simulation states at peak strain for corpus callosum, gray matter and white matter.

5.4 Risk estimates - Rib fractures

CIREN and NASS-CDS database injury descriptions of the thorax for the selected cases can be roughly categorized into three severity types: fractured ribs, minor injury severity and non-injury, as illustrated in Figure 5.3. It is known that three cases out of 11 (27 %) have sustained multiple rib fractures. The average estimated AIS2+ risk of the 11 reconstructed cases is roughly 50 %, according to Table 4.2. Thus, 11·0.5=5.5 occupants are according to obtained results expected to get at least two fractured ribs, when in reality three occupans were detected to have fractures at AIS2+ level. This indicates that obtained probability is in overall overpredicted. However, due to limited number of reconstruction cases, this is considered not to be a very accurate indication. Due to the individual variations (different occupants from the selected cases might have abnormal injury tolerance), it should neither be expected that each individual case matches the real-world injury outcome.

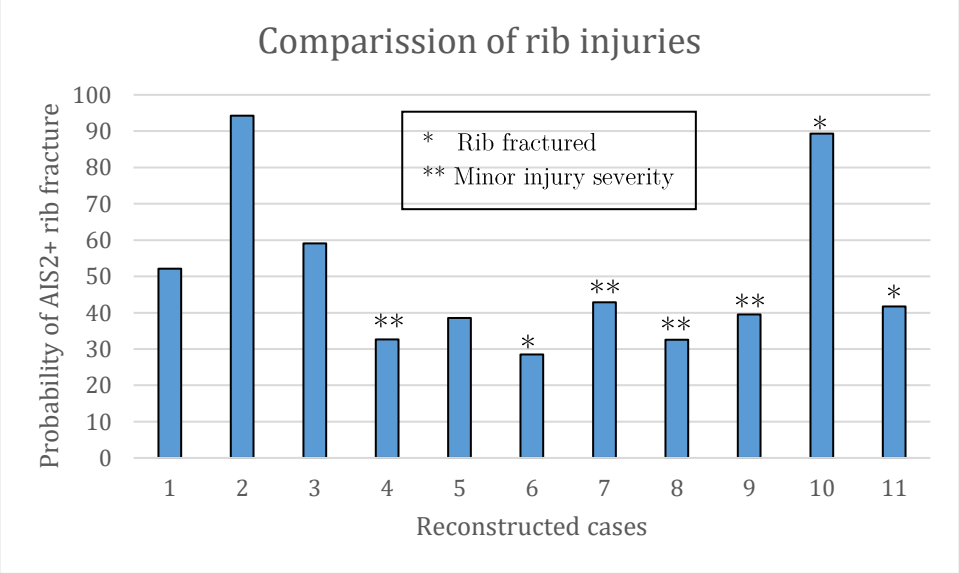

Figure 5.3: Probability of getting AIS2+ rib fracture in the 11 reconstructed cases, compared with the cases extracted from the databases which sustained rib fracture (*) or minor injury severity (**)

When looking at the estimations for individual cases it is apparent that case 2 and 10 stands out with the highest probability values. This could be expected for case 10, which has multiple rib fractures reported. However, case 2 represent a

mismatch to the real-world injury outcome. For the cases in the non-injury category, a probability much closer to zero was expected.

In order to increase the possibility of obtaining a correlation with better fit, it is desirable to add more reconstruction cases to the current reconstructions. In addition, morphing of the model could be implemented for further improved of the rib fracture injury prediction. The morphing accounts for human's deviation from the averaged sized male and is controlled by several independent parameters such as body mass index (BMI), age and sex. Several studies, such as [14], [73] and [74] have in recent time implemented morphing, where it was reported that the morphing of the model had some influence on the results.

5.5 Risk estimates – Lumbar spine

As it has been pointed out in the literature overview, estimation of AIS2+ lumbar fractures need more attention. The analysis of lumbar spine fractures in this study was conducted with the purpose to increase the understanding of forces and moments generated in lumbar vertebral during vehicle collision accidents.

The results from the implemented $L_{index,C}$ criterion indicate that the highest risk for rib fractures is most probable for vertebrae L4-L5. However, the majority of the reported real-world lumbar fractures of the reconstructed cases occurred in L1-L3 vertebrae. Intuitevely, it is reasonable that L5 level is subjected to the largest loading due to the greater support of the body weight compared to the upper lumbar vertebrae. This is also the reason why lumbar vertebrae are larger in size compared to the vertebra levels in the rest of the spine. However, it is worth mentioning that $L_{index,C}$ is a global criterion, meaning that results are not accounting the variable lumbar vertebra sizes and consequenstly not taking into account the variable strength of each vertebrae. Thus, it is difficult to achieve a proper match on vertebra specific results.

$L_{index,C}$ of 1 corresponds to a 50 % risk for fracture based on the intercept values, which would mean that $0.5 \cdot 11 = 5.5$ occupants have lumbar fracture, which is close to the actual outcome where 6 occupants had lumbar fracture. However, the obtained average maximum $L_{index,C}$ value is only 0.52 (see Table 4.3), which means that injury outcome is underestimated on a population level.

The lumbar spine criterion has been implemented based on the previous studies. Since there are no widely accepted criteria for lumbar spine injury assessment, several assumptions had to be made in order to relate measured forces and moments to the reported real-world injury outcomes. One of the assumptions is that the criteria should be based on compressive forces only, in axial loading. Tension forces have been excluded due to considering that the used thresholds were based on compression fractures. Another assumption that has been made is to consider the forces and moments that occur at the same time, instead of choosing peak values of the loads independently of the time history. If the peak values have been considered instead, it would be reasonable to expect higher probability index values.

As one attempt to improve the prediction of injury probability, the effect of age adjustment of $L_{index,C}$ should be explored. According to [75] and [76], age represent an increased risk of lumbar fractures, with a yearly increased fractured odds by four percent. In addition, morphing of the model is supposed to have a certain effect on the results, similarly as for the thorax. However, it should be kept in mind that in this study, $L_{index,C}$ criteria is assumed to be valid based extensively on the 50 percentile average male model as it can be speculated that the injury tolerance will change with the changed size of the vertebra bodies. Thus, the results have been reported only based on unscaled models, which might have affected the results for the cases 1-2 and 6-7 due to somewhat mismatched postures.

Another possible way to estimate lumbar spine fractures without having a certain index criterion, is by considering the individual loads measured in the lumbar spine. In Stamper [71], lumbar spine injury risks based on compressive force with 95% confidence interval is presented, from where it can be seen that $F_{z,crit} = 4.5$ kN corresponds to 50 % probability fracture risk. The maximum reported compression force in this study is 1.962 kN (see Figure 4.5), which corresponds to an injury probability risk less than 10 %. With this in mind, it becomes obvious that the measured compressive forces alone are not high enough to be considered as a threat of causing the injury.

6 Conclusion

Based on the estimated probability risk, it can be conluded that the model do not predict the concussion outcome when considering individual cases where concussion is expected due to reported severe head injuries. The obtained trend indicates that the model significantly underestimates the probability for concussion.

The preliminary conclusion from the evaluated risk for AIS2+ chest injuries is that the model overpredicts the rib fracture probability. Although a matching trend is found in several of the cases, when considering the overall results, a desirable match with the real-world injury is not achieved. However, it is considered that the model's validity can not be concluded based on obtained results on their own. For this reason, it is necessary to simulate more cases.

Assessment of measured loads on the lumbar spine revealed that the forces and moments on their own are fairly low to present a threat of compression fracture vertebral injury. The highest compression forces are observed in L4-L5 vertebral level. This eventually results in an un-matched estimated probability based on the applied lumbar spine injury criterion when comparing to the reported real-world injuries of the corresponding cases. The implemented $\mathsf{L}_{\mathsf{index,C}}$ criterion is considered to serve as a preliminary step for assessment of compression fracture to the vertebrae.

7 Future work

One future study recommendation would be to re-run the simulations with morphed SAFER HBMs. By incorporating morphing, a model with a better representation of specific occupant's anthropometrics would be obtained, taking into account gender differences and a greater variety of statures. This could clarify whether and how much the geometrically morphed models contribute to injury prediction of a wider population range.

The spinal injury validation would be more convenient with age-adjusted version of the lumbar spine injury criterion by which bone mineral density variations are accounted, as it has been proposed in studies [9] and [67] etc. Moreover, it is desirable to complement spinal injury assessment with stress and strain metrics by relating the peak values with the real-world injury outcomes. With these metrics, the validation of the spine injury could also be extended to thoracic region in order to obtain a more complete spinal injury validation. Findings from the literature overview indicates that the most frequently injured vertebras are the ones that are located in the transition region between the thoracic and lumbar region.

When it comes to the concussion evaluation, a question mark remains regarding whether or not the performed vehicle reconstructions are a suitable method for concussion validation, due to the less controlled boundary conditions of the head. One suggestion for future work is to validate concussion based on the real-world injury accidents with well-reported head kinematics, which would serve as specific input values to the FE model. Having more controlled head kinematic is expected to diminish current uncertainties regarding concussion assessment.

To additionally reduce uncertainties, new case selection should be considered with more clear injury concussion indications. The cases where concussion is not examined (NFS) should be avoided. In overall, making the sample more balanced with injured/uninjured cases would be desirable for all of the considered injury estimations.

References

[1] "Global status report on road safety 2018. Geneva: World Health Organization;," 2018.

[2] S. Kleiven, "Predictors for Traumatic Brain Injuries Evaluated through Accident Reconstructions," *SAE Tech. Pap.*, vol. 2007-Octob, no. October, 2007, doi: 10.4271/2007-22-0003.

[3] J. Iraeus and B. Pipkorn, "Development and Validation of a Generic Finite Element Ribcage to be used for Strain-based Fracture Prediction," *Proc. IRCOBI Conf.*, no. September, pp. 193–210, 2019.

[4] J. Östh, M. Mendoza-Vazquez, A. Linder, M. Y. Svensson, and K. Brolin, "The VIVA OpenHBM finite element 50th percentile female occupant model: Whole body model development and kinematic validation," *Conf. Proc. Int. Res. Counc. Biomech. Inj. IRCOBI*, vol. 2017-Septe, pp. 443–466, 2017.

[5] B. Pipkorn, "Multi-Scale Validation of a Rib Fracture Prediction Method for Human Body Models," *Ircobi*, vol. 46, no. 0, 2019.

[6] J. Iraeus *et al.*, "Detailed subject-specific FE rib modeling for fracture prediction Detailed subject-specific FE rib modeling for fracture prediction," *Traffic Inj. Prev.*, 2019, doi: 10.1080/15389588.2019.1665649.

[7] "About SAFER | SAFER – Vehicle and Traffic Safety Centre at Chalmers." [Online]. Available: https://www.saferresearch.com/about. [Accessed: 29-May-2020].

[8] X. Ye *et al.*, "Numerical investigation of driver lower extremity injuries in finite element frontal crash reconstruction," *Traffic Inj. Prev.*, vol. 19, pp. S21–S28, 2018, doi: 10.1080/15389588.2017.1376051.

[9] X. Ye, J. P. Gaewsky, D. A. Jones, L. E. Miller, J. D. Stitzel, and A. A. Weaver, "Computational modeling and analysis of thoracolumbar spine fractures in frontal crash reconstruction," *Traffic Inj. Prev.*, vol. 19, no. sup2, pp. S32–S39, 2018, doi: 10.1080/15389588.2018.1498090.

[10] J. Iraeus and M. Lindquist, "Development and validation of a generic finite element vehicle buck model for the analysis of driver rib fractures in real

life nearside oblique frontal crashes," *Accid. Anal. Prev.*, vol. 95, pp. 42–56, 2016, doi: 10.1016/j.aap.2016.06.020.

[11] D. Jones, J. Gaewsky, A. Weaver, and J. Stitzel, "A Semi-Automated Approach to Real World Motor Vehicle Crash Reconstruction Using a Generic Simplified Vehicle Buck Model," *SAE Int. J. Transp. Saf.*, vol. 4, no. 2, 2016, doi: 10.4271/2016-01-1488.

[12] "Injuries associated with airbag deployment," doi: 10.1136/emj.19.6.490.

[13] "Universal Emark Certificated Three Points Car Safety Seat Belt Retractor." [Online]. Available: https://www.autocarseatbelt.com/3-point-seat-belt.html. [Accessed: 02-Jun-2020].

[14] B. Pipkorn, J. Iraeus, M. Björklund, O. Bunketorp, and L. Jakobsson, "Multi-Scale Validation of a Rib Fracture Prediction Method for Human Body Models," *Proc. IRCOBI Conf.*, no. 0, pp. 175–192, 2019.

[15] M. Fahlstedt, *Numerical Accident Reconstructions A Biomechanical Tool to Understand and Prevent Head Injuries*. .

[16] "LS-DYNA | Livermore Software Technology Corp." [Online]. Available: https://www.lstc.com/products/ls-dyna. [Accessed: 29-May-2020].

[17] J. O. Hallquist, "LS-DYNA ® THEORY MANUAL," 2006.

[18] "ANSA pre-processor - BETA CAE Systems." [Online]. Available: https://www.beta-cae.com/ansa.htm. [Accessed: 29-May-2020].

[19] "BETA CAE Systems - META post-processor." [Online]. Available: https://www.beta-cae.com/meta.htm. [Accessed: 29-May-2020].

[20] L. W. Schneider et al., "Biotab-a new method for analyzing and documenting injury causation in motor-vehicle crashes," *Traffic Inj. Prev.*, vol. 12, no. 3, pp. 256–265, 2011, doi: 10.1080/15389588.2011.560500.

[21] "How It Works: Crash reconstruction | Driving." [Online]. Available: https://driving.ca/auto-news/news/how-it-works-crash-reconstruction. [Accessed: 29-May-2020].

[22] "Crash Injury Research and Engineering Network | Wake Forest School of Medicine." [Online]. Available: https://school.wakehealth.edu/Departments/Biomedical-

Engineering/Center-for-Injury-Biomechanics/Crash-Injury-Research-and-Engineering-Network. [Accessed: 29-May-2020].

[23] X. yun Zhang, X. long Jin, W. guo Qi, and Y. zhi Guo, "Virtual reconstruction of vehicle crash accident based on elastic-plastic deformation of auto-body," *Adv. Eng. Softw.*, vol. 39, no. 6, pp. 459–465, 2008, doi: 10.1016/j.advengsoft.2007.05.002.

[24] S. Evtiukov, E. Golov, and G. Ginzburg, "Finite element method for reconstruction of road traffic accidents," *Transp. Res. Procedia*, vol. 36, pp. 157–165, 2018, doi: 10.1016/j.trpro.2018.12.058.

[25] "Crash Injury Research | NHTSA." [Online]. Available: https://www.nhtsa.gov/research-data/crash-injury-research. [Accessed: 29-May-2020].

[26] J. P. Gaewsky, A. A. Weaver, B. Koya, and J. D. Stitzel, "Driver Injury Risk Variability in Finite Element Reconstructions of Crash Injury Research and Engineering Network (CIREN) Frontal Motor Vehicle Crashes," *Traffic Inj. Prev.*, vol. 16, no. October, pp. 124–131, 2015, doi: 10.1080/15389588.2015.1061666.

[27] D. J. Gabauer and H. C. Gabler, "Comparison of delta-V and occupant impact velocity crash severity metrics using event data recorders," *Annu. Proc. - Assoc. Adv. Automot. Med.*, vol. 2006, pp. 57–71, 2006.

[28] J. Iraeus and M. Lindquist, "Analysis of Delta Velocity and PDOF by Means of Collision Partner and Structural Involvement in Real-Life Crash Pulses With Modern Passenger Cars," *Traffic Inj. Prev.*, vol. 15, no. 1, pp. 56–65, 2014, doi: 10.1080/15389588.2013.793796.

[29] T. Xu, X. Sheng, T. Zhang, H. Liu, X. Liang, and A. Ding, "Development and validation of dummies and human models used in crash test," *Appl. Bionics Biomech.*, vol. 2018, 2018, doi: 10.1155/2018/3832850.

[30] S. Y. Hsu *et al.*, "Impact of Adapting the Abbreviated Injury Scale (AIS)-2005 from AIS-1998 on Injury Severity Scores and Clinical Outcome.," *Int. J. Environ. Res. Public Health*, vol. 16, no. 24, p. 5033, 2019.

[31] "Abbreviated Injury Scale (AIS) - Association for the Advancement of Automotive Medicine." [Online]. Available: https://www.aaam.org/abbreviated-injury-scale-ais/. [Accessed: 29-Apr-

2020].

[32] Kai-Uwe S., P. F. Niederer, M. H. Muser, and F. Walz, *Trauma Biomechanics - Accident Injury in Traffic and Sports*, 3:rd editi. Springer, 2009.

[33] Jakobsson L., B. M., and W. A., "Thoracolumbar spine injuries in car crashes," *IRCOBI Conf. Proc. - Int. Res. Counc. Biomech. Inj.*, pp. 101–112, 2016.

[34] "Motor-Vehicle Crash Reconstruction Services." [Online]. Available: http://www.crashforensics.com/crashreconstruction.cfm. [Accessed: 29-May-2020].

[35] J. Iraeus and M. Lindquist, "Development and validation of a generic finite element vehicle buck model for the analysis of driver rib fractures in real life nearside oblique frontal crashes," *Accid. Anal. Prev.*, vol. 95, pp. 42–56, 2016, doi: 10.1016/j.aap.2016.06.020.

[36] M. Mendoza-Vazquez, L. Jakobsson, J. Davidsson, and E. Al., "Evaluation of Thoracic Injury Criteria for THUMS Finite Element Human Body Model Using Real-World Crash data," 2014.

[37] A. J. Golman, K. A. Danelson, L. E. Miller, and J. D. Stitzel, "Injury prediction in a side impact crash using human body model simulation," *Accid. Anal. Prev.*, vol. 64, pp. 1–8, 2014, doi: 10.1016/j.aap.2013.10.026.

[38] "File:Blausen 0110 BrainLayers.png - Wikimedia Commons." [Online]. Available: https://commons.wikimedia.org/wiki/File:Blausen_0110_BrainLayers.png. [Accessed: 31-May-2020].

[39] Y. Pinto *et al.*, "Split brain: Divided perception but undivided consciousness," *Brain*, vol. 140, no. 5, pp. 1231–1237, 2017, doi: 10.1093/brain/aww358.

[40] "Corpus callosum - Queensland Brain Institute - University of Queensland." [Online]. Available: https://qbi.uq.edu.au/brain/brain-anatomy/corpus-callosum. [Accessed: 29-May-2020].

[41] A. A. Mercadante and P. Tadi, *Neuroanatomy, Gray Matter*. StatPearls Publishing, 2020.

[42] R. D. Fields, “Change in the brain’s white matter,” *Science*, vol. 330, no. 6005. NIH Public Access, pp. 768–769, 05-Nov-2010, doi: 10.1126/science.1199139.

[43] “File:Brain Anatomy (Sagittal).png - Wikimedia Commons.” [Online]. Available: https://commons.wikimedia.org/wiki/File:Brain_Anatomy_(Sagittal).png. [Accessed: 31-May-2020].

[44] C. Deck and R. Willinger, “Improved head injury criteria based on head FE model,” *Int. J. Crashworthiness*, vol. 13, no. 6, pp. 667–678, 2008, doi: 10.1080/13588260802411523.

[45] K. M. Tse, S. P. Lim, V. B. C. Tan, and H. P. Lee, “A review of head injury and finite element head models,” *Am. J. Eng.*, vol. 1, no. 5, pp. 28–52, 2014.

[46] D. R. G. Ellenbogen, L. N. Sekhar, and N. Kitchen, *Principles of Neurological Surgery*, 4th ed. 2018.

[47] B. McHenry, “Head injury criterion and the ATB,” *ATB Users’ Gr.*, no. February, pp. 5–8, 2004.

[48] “File:Coup injury.jpg - Wikimedia Commons.” [Online]. Available: https://commons.wikimedia.org/wiki/File:Coup_injury.jpg. [Accessed: 02-Jun-2020].

[49] F. A. O. Fernandes, R. J. Alves De Sousa, and M. Ptak, *Head Injury Simulation in Road Traffic Accidents*. SPRINGER BRIEFS IN APPLIED SCIENCES AND TECHNOLOGY, 2018.

[50] A. C. Bain and D. F. Meaney, “Tissue-Level Thresholds for Axonal Damage in an Experimental Model of Central Nervous System White Matter Injury,” *ASME. J Biomech Eng.*, vol. 122, no. 6, pp. 615–622, 2000.

[51] L. E. Thibault, “Brain injury from the macro to the micro level and back again: What have we learned to date?,” in *Proc. IRCOBI Conf*, 1993, p. pps. 3-25.

[52] J. L. Forman, R. W. Kent, K. Mroz, B. Pipkorn, O. Bostrom, and M. Segui-Gomez, “Predicting rib fracture risk with whole-body finite element models: Development and preliminary evaluation of aprobabilistic

analytical framework," in *Annals of Advances in Automotive Medicine*, 2012, vol. 56, pp. 109–124.

[53] W. J. Hamilton, *Textbook of Human Anatomy*. The Macmillan Press LTD, 1976.

[54] Institute of Medicine and National Research Council, *Injury in America: A Continuing Public Health Problem*. National Academies Press, 1985.

[55] M. Mendoza-Vazquez, J. Davidsson, and K. Brolin, "Construction and evaluation of thoracic injury risk curves for a finite element human body model in frontal car crashes," *Accid. Anal. Prev.*, vol. 85, pp. 73–82, 2015, doi: 10.1016/j.aap.2015.08.003.

[56] K. U. Schmitt, P. F. Niederer, D. S. Cronin, B. Morrison III, M. H. Muser, and F. Walz, *Trauma biomechanics: an introduction to injury biomechanics.* 2019.

[57] "File:725 Lumbar Vertebrae.jpg - Wikimedia Commons." [Online]. Available: https://commons.wikimedia.org/wiki/File:725_Lumbar_Vertebrae.jpg. [Accessed: 01-Jun-2020].

[58] "File:Gray94.png - Wikimedia Commons." [Online]. Available: https://commons.wikimedia.org/wiki/File:Gray94.png. [Accessed: 31-May-2020].

[59] D. M. Stein, J. A. Kufera, S. M. Ho, G. E. Ryb, P. C. Dischinger, and J. V. O'Connor, "Occupant and crash characteristics for case occupants with cervical spine injuries sustained in motor vehicle collisions," *Scalea TM J Trauma*, vol. 70, no. 2, pp. 299–309, 2011.

[60] F. A. Pintar, N. Yoganandan, D. J. Maiman, M. Scarboro, and R. W. Rudd, "Thoracolumbar spine fractures in frontal impact crashes," *Ann Adv Automot Med.*, vol. 56, pp. 277–283, 2012.

[61] P. Begeman, A. King, and P. Prasad, "Spinal loads resulting from -gx acceleration," in *Proc 17th Stapp Car Crash Conf., SAE 730977*, 1973, pp. 33–360.

[62] H. Mertz and L. Patrick, "Strength and response of the human neck," in *Proc. 15th Stapp Car Crash Conf., SAE 710 855*, 1971, pp. 207–255.

[63] H. Mertz and L. Patrick, "Investigation of the kinematics and kinetics whiplash," in *Proc. 11th Stapp Car Crash Conf., SAE 670 919*, 1971, pp. 2952–2980.

[64] K. Ono, S. Ejima, Y. Suzuki, K. Kaneoka, M. Fukushima, and S. Ujihashi, "Prediction of neck injury risk based on the analysis of localized cervical vertebral motion of human volunteers during low-speed rear impacts," in *Proc. IRCOBI Conf.*, 2006, pp. 103–113.

[65] T. H. Hansson, T. S. Keller, and M. M. Panjabi, "A study of the compressive properties of lumbar vertebral trabeculae: effects of tissue characteristics," *Spine (Phila Pa 1976)*, vol. 12, pp. 56–62, 1987.

[66] DENIS, FRANCIS, MD, and FRCS(C), "The Three Column Spine and Its Significance in the Classification of Acute Thoracolumbar Spinal Injuries," vol. 8, no. 8, pp. 817–831, 1983.

[67] N. Yoganandan, M. W. Arun, B. D. Stemper, F. A. Pintar, and D. J. Maiman, "Biomechanics of human thoracolumbar spinal column trauma from vertical impact loading," *Ann Adv Automot Med*, vol. 57, pp. 155–166, 2013.

[68] J. González, M. Wiberg, and A. A. von Davier, "A note on the Poisson's binomial distribution in item response theory," *Appl. Psychol. Meas.*, vol. 40, no. 4, pp. 302–310, 2016.

[69] J. Iraeus and M. Lindquist, "Analysis of minimum pulse shape information needed for accurate chest injury prediction in real life frontal crashes Analysis of minimum pulse shape information needed for accurate chest injury prediction in real life frontal crashes," *Int. J. Crashworthiness*, 2020, doi: 10.1080/13588265.2020.1769004.

[70] "Surface vehicle recommendet practice. Instrumentation for impact test - Part 1," *Electron. Instrum. SAE Int. J211-1*, 1970.

[71] B. D. Stemper and et Al., "Biomechanical tolerance of whole lumbar spines in straightened posture subjected to axial acceleration," *J. Orthop. Res.*, vol. 36, no. 6, pp. 1747–1756, 2018, doi: 10.1002/jor.23826.

[72] A. Belwadi and K. H. Yang, "Response of the cadaveric lumbar spine to flexion with and without anterior shear displacement," in *Int. Res. Counc. Biomech. Inj. - 2008 Int. IRCOBI Conf. Biomech. Inj. Proc.*, 2008, pp. 397–

410.

[73] K. Zhang, L. Cao, A. Fanta, and et al., "An automated method to morph finite element whole-body human models with a wide range of stature and body shape for both men and women.," *J. Biomech. 60*, pp. 253–260, 2017.

[74] Y. Wang, L. Cao, Z. Bai, and E. Al., "A parametric ribcage geometry model accounting for variations among the adult population," *J. Biomech. 49(13)*, pp. 2791–2798, 2016.

[75] L. Bilston, E. Clarke, and J. Brown, "Spinal injury in car crashes: crash factors and the effects of occupant age.," *Inj Prev*, vol. 17, pp. 228–232, 2011.

[76] R. Kaufman, R. Ching, M. Willis, C. Mack, J. Gross, and E. Bulger, "Burst fractures of the lumbar spine in frontal crashes.," *Accid Anal Prev*, vol. 59, pp. 153–163, 2013.

Appendix

A. Posture of the SAFER HBM

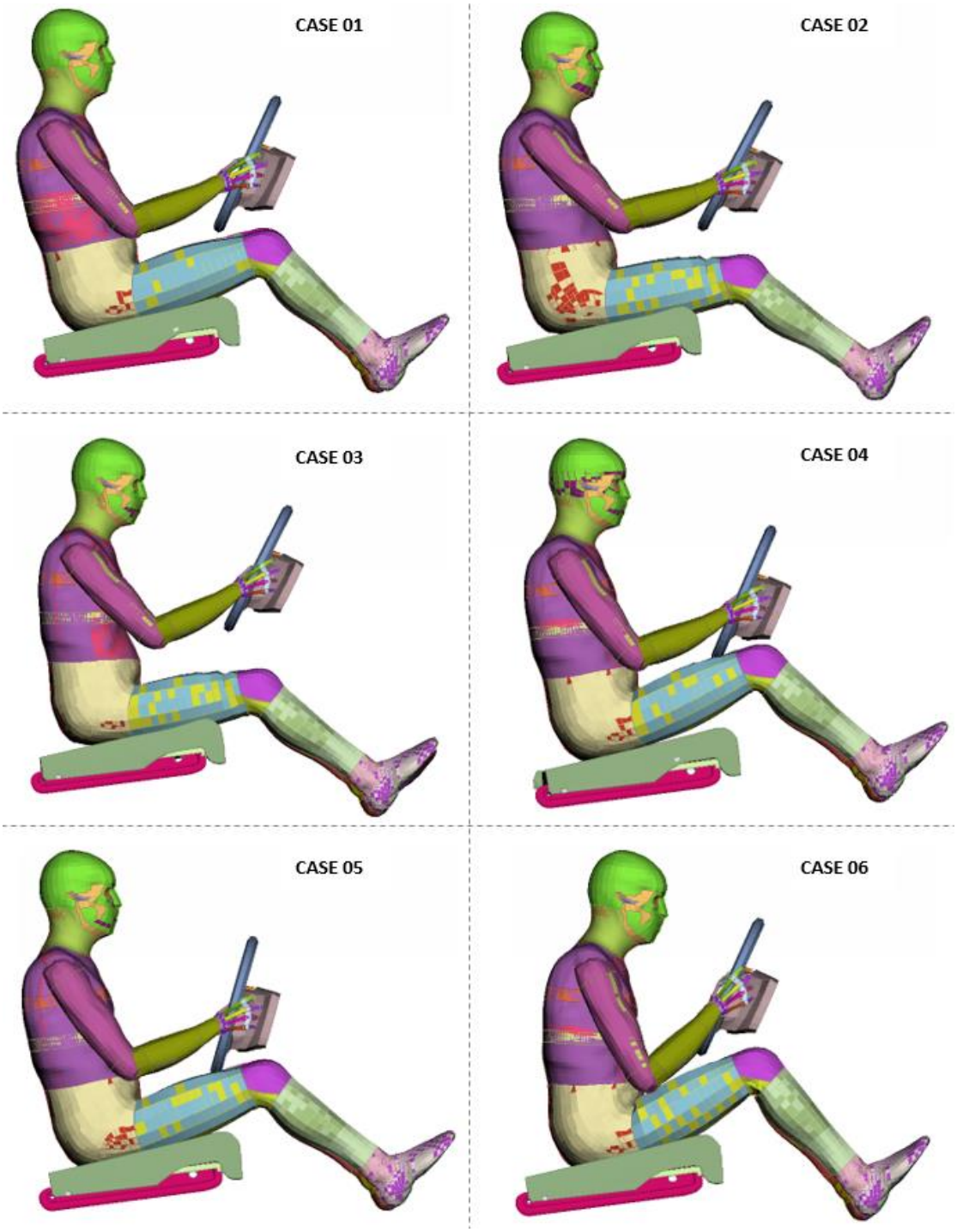

Figure A.0.1: Posture of the SAFER HBM v9 for (unscaled) cases 1-6.

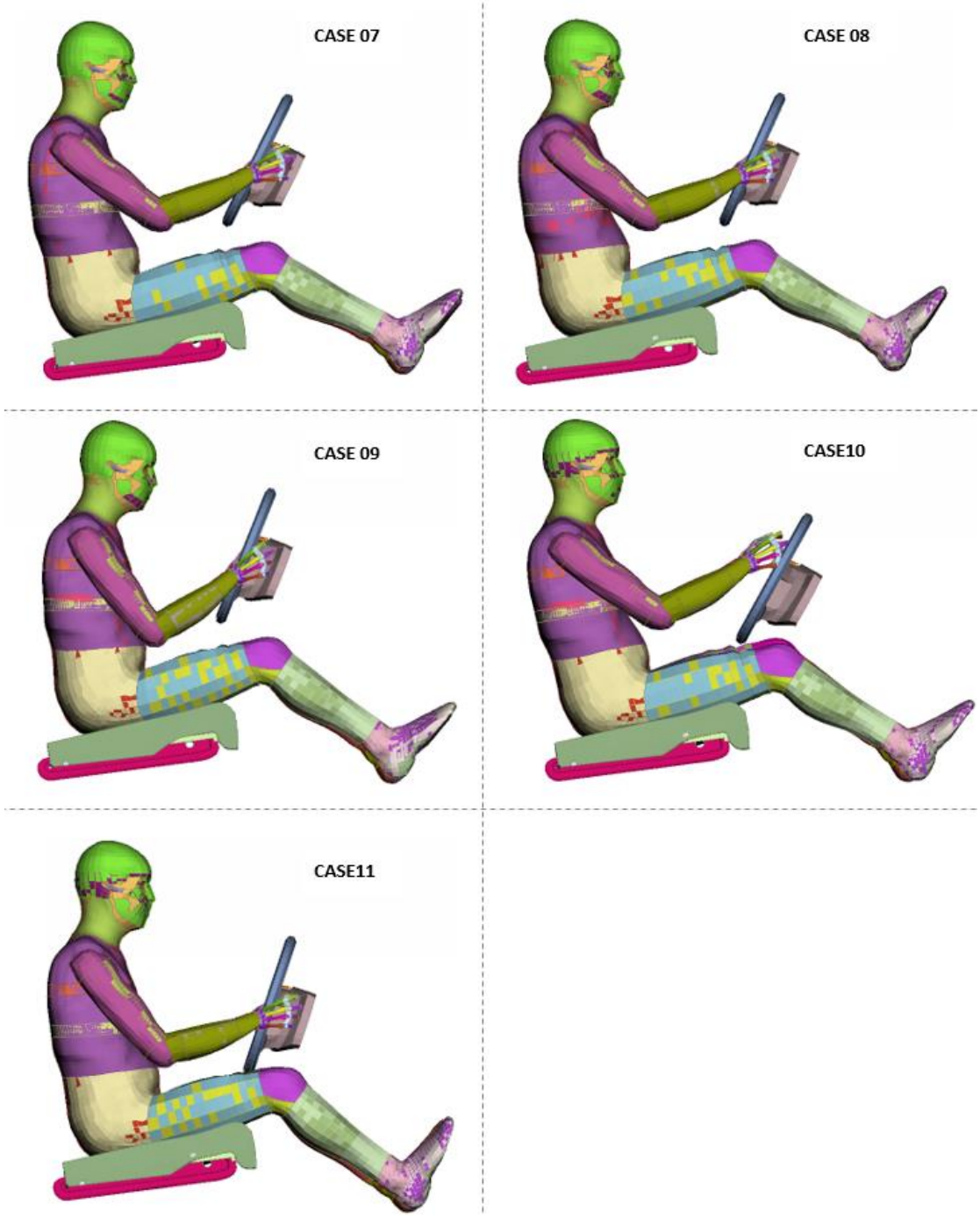

Figure A.0.2: Posture of the SAFER HBM v9 for (unscaled) cases 7-11.

B. Risk curves for concussion estimation

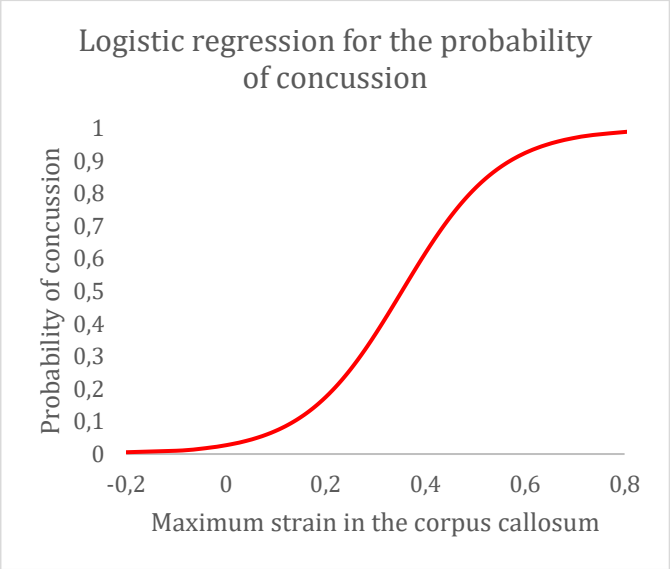

Figure B.0.3: Logistic regression risk curve for the probability of AIS2+ concussion based on corpus callosum (graph is recreated based on Kleiven [2]).

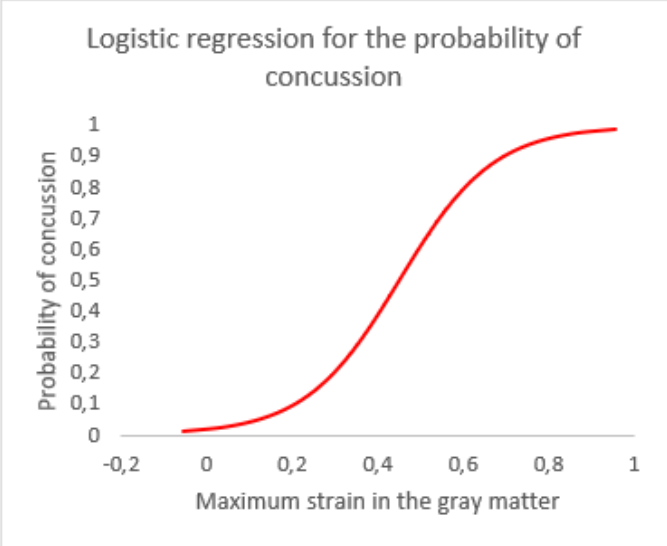

Figure B.0.4: Logistic regression risk curve for the probability of AIS2+ concussion based on gray matter (graph is recreated based on Kleiven [2]).

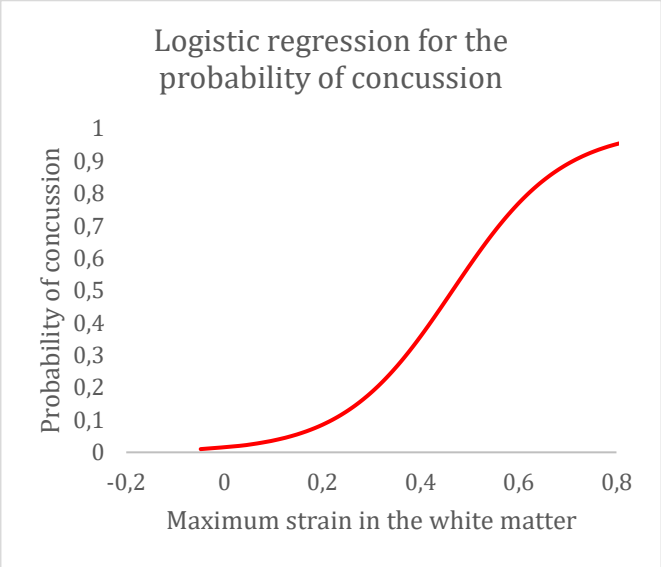

Figure B.0.5: Logistic regression risk curve for the probability of AIS2+ concussion based on white matter (graph is recreated based on Kleiven [2]).

C. R-script

```
# AIS2p.R:
library (MASS)
library (poibin)
chest_ribprob_AIS2p<-function(runname,strainvector,age) {
# number of ribs considered
noribs<-length(strainvector)
# Baseline strain to fracture curve for 25y male
microstrain_25y<-
c(16571.73256,20123.02106,21213.61868,22304.33154,23866.85089,29803.69958,32
115.52818,32907.92136,34340.52338,35913.83981,40906.0056,41123.05122)
# Transform curve to current AGE
microstrain_age<-microstrain_25y
for (i in (1:length(microstrain_25y))) {
microstrain_age[i]<-(1-((age-25)*0.0051))*microstrain_25y[i]
}
# Fit Weibull distribution
distparam<-fitdistr(microstrain_age,"weibull")
# Compute fracture probability for each rib
rib_prob<-rep(0.0, noribs)
for (i in (1:noribs)) {
  rib_prob[i]<-
pweibull(1000000*strainvector[i],distparam$estimate[1],distparam$estimate[2]
)
}
# Compute pdf for combined probability for chest
pdf_age<-dpoibin(0:noribs, rib_prob)
# Compute risk for AIS2+
AIS2p_age<-1-pdf_age[1]-pdf_age[2]
# print(c(runname, AIS3p_age))
return(AIS2p_age) }
#
```

CHALMERS
UNIVERSITY OF TECHNOLOGY